

A Navigation Solution Using a MEMS IMU, Model-Based Dead-Reckoning, and One-Way-Travel-Time Acoustic Range Measurements for Autonomous Underwater Vehicles

James H. Kepper IV , Member, IEEE, Brian C. Claus, Member, IEEE, and James C. Kinsey, Member, IEEE

Abstract—Recent advances in acoustic navigation methods are enabling extended autonomous underwater vehicles’ (AUVs) mission time while maintaining their XY position error within appropriate limits. Furthermore, while advances in inertial sensor technology are drastically lowering the size, power consumption, and cost of these sensors, these sensors remain noisy and accrue error over time. This paper builds on the research and recent developments in single beacon one-way-travel-time acoustic navigation and investigates the degree of bounding position error for small AUVs with a minimal navigation strapdown sensor suite, relying on a consumer grade microelectromechanical system inertial measurement unit (IMU) and a vehicle’s dynamic model velocity. An implementation of an extended Kalman filter that includes IMU bias estimation and coupled with a range filter is obtained in the field on two types of AUVs. Results from these field trials in controlled environments and ocean show that the reported navigation solution possesses an accuracy comparable to existing methods.

Index Terms—Autonomous underwater vehicle (AUV), Kalman filter, microelectromechanical systems (MEMS) inertial measurement unit (IMU), navigation, one-way travel time (OWTT).

I. INTRODUCTION

PROGRESS in underwater robotic systems continues to expand our observational capabilities in the ocean in a variety of domains including in the oceanographic research and military communities. Navigation is an area of particular focus in the underwater robotics community as the rapid attenuation of

Manuscript received September 19, 2017; revised February 8, 2018; accepted April 29, 2018. Date of publication June 20, 2018; date of current version July 12, 2019. This work was supported in part by the U.S. Navy’s Civilian Institution program via the MIT/WHOI Joint Program, in part by the WHOI Postdoctoral Scholar program, in part by the Keck Institute for Space Studies, and in part by the Woods Hole Oceanographic Institution. This work was presented in part at the IEEE/MTS OCEANS Conference, Aberdeen, Scotland, June 19–22, 2017. (*Corresponding author: James H. Kepper.*)

Associate Editor: B. Englöt.

J. H. Kepper, IV, was with the MIT/WHOI Joint Program, Woods Hole Oceanographic Institution, Woods Hole, MA 02543 USA. He is now with U.S. Navy, Washington, DC 20350 USA (e-mail: jkepper@whoi.edu).

B. C. Claus is with the Woods Hole Oceanographic Institution, Woods Hole, MA 02543 USA (e-mail: bclaus@whoi.edu).

J. C. Kinsey is with the Woods Hole Oceanographic Institution, Woods Hole, MA 02543 USA (e-mail: jkinsey@whoi.edu).

Digital Object Identifier 10.1109/JOE.2018.2832878

radio frequency signals in water precludes using the global positioning system (GPS) on submerged robots—thus, alternative methods must be used [1], [2]. Strapdown navigation techniques, such as inertial navigation systems (INSs) and Doppler velocity logs (DVLs) (e.g., [3]–[5]) are used on many robots; however, these methods still require aiding from external navigation sensors that provide absolute position estimates. Acoustic methods, such as long baseline (LBL) [6] and ultrashort baseline (USBL) [7], provide aiding for deeply submerged robots; however, each possesses unique infrastructure constraints. Furthermore, these solutions scale poorly to multiple autonomous underwater vehicle (AUV) operations because the update rate must be divided by the number of available vehicles. The necessity for multiple AUV operations is motivated by a growing number of observational challenges that require simultaneous coordinated surveying from multiple ocean robots—examples include sampling of nested heterogeneous ocean processes [8], autonomous hydrothermal exploration [9], [10], and characterization of biological and evolutionary hotspots in remote ocean regions [11]. Work over the past decade in one-way travel time (OWTT) (e.g., [12]–[18]) has developed acoustic methods that scale to these emerging operational needs; however, OWTT methods require an independent source of odometry, such as DVLs (which cost \$20 000–\$40 000) or, as reported in [19] and [20], estimates of the robot’s odometry from models of the robots dynamics.

Herein, we report a navigation solution based on a microelectromechanical systems (MEMS) inertial measurement unit (IMU), a vehicle’s dynamic model velocity, and acoustic time-of-flight (TOF) range measurements from an OWTT navigation system. An implementation of an extended Kalman filter (EKF) that includes IMU bias estimation is reported and validated using field experiments from three different field locations—the first two in controlled environments and a third in open water off the California coast. Results from these experiments show that the navigation solution accuracy is comparable to current standard navigation methods. These results build on prior work reported in [21] and, to the best of our knowledge, these papers report the first results that fuses odometry estimates from an IMU with OWTT navigation.

The remainder of this paper is organized as follows. The remainder of this section briefly reviews previously reported work in OWTT and inertial navigation. Section II presents the models used in our EKF formulation. Our experimental configuration is reported in Section III. Sections IV and V present experimental results. Section VI provides concluding remarks.

A. Background

1) Acoustic TOF Navigation: GPS provides land, air, and sea surface robots with highly accurate and absolute position measurements; thus enabling highly accurate navigation solutions. However, for robots operating underwater, the lack of GPS signals poses unique challenges. AUVs typically navigate by means of various sensors to compute a dead-reckoned (DR) odometry [1], [2]. However, without external aiding, position error grows unbounded over time.

AUVs can surface periodically to obtain GPS measurements; thus updating position estimates and reducing its error. However, periodic surfacing limits the energy consumption efficiency (thus reducing its overall mission time) and inhibits covert missions needed for military applications, and, for deep-diving AUVs, periodic surfacing requires they leave the areas of interest. One such solution for providing absolute position measurements while the vehicle remains submerged is acoustic TOF navigation. LBL navigation [6], in which an AUV triangulates its position to fixed surveyed acoustic transponders, requires time-consuming surveys (with the attendant expensive ship time) while limiting the mission coverage area. USBL navigation [7] is an alternative method that does not require to fixed transponders on the ocean bottom, but it still requires the ship, with its expensive operational time, to remain on station and precludes conducting simultaneous missions in different areas. Additionally, fusing USBL position data with the AUV's on-board navigation solution requires the ship to transmit the USBL position via acoustic packets to the AUV, which often results in latency [22].

Advances in single-beacon acoustic navigation over the past decade present an alternative means for bounding XY navigation error (the Z degree of freedom is of less concern as depth is measured by pressure depth sensors). In this method, a surface beacon, which has access to the GPS, transmits its position to a submerged vehicle in an acoustic packet. Highly accurate and synchronized clocks (a chip-scale atomic clock (CSAC) or a temperature-compensated crystal oscillator coupled with a pulse-per-second clock) [23], [24] on both the beacon and the receiving vehicle accurately measure the acoustic packet's OWTT TOF. From this TOF calculation, a range between the surface beacon and the vehicle is determined using measurements of the water column's sound velocity, and this range is used to constrain the AUV's position estimate; thus bounding its XY position error. Many successful experimental results using single-beacon OWTT range measurements over the past decade prove this capability of bounding position error [12]–[18]. More recently, a moving short baseline navigation solution that incorporated two transducers on the surface beacon made use of OWTT range constraints [25]. For this method, when the AUVs are distant from the surface ship, the two surface beacons act as a single beacon providing OWTT range measurements. However,

when the AUVs are near the surface beacon, navigation and localization improve due to the two transponders. These results incorporate a variety of state estimation algorithms, primarily consisting of position displacement odometry determined by a DVL, which is constrained by the OWTT range measurements. The major advantage for single-beacon OWTT navigation, in addition to constraining submerged XY position, is the ability to deploy multiple vehicles that each simultaneously receive position data acoustic packets from the same surface beacon, and hence, the position update rate for each vehicle remains constant.

Observability is important with range-only measurement methods. Since a range measurement only provides a constraint and not an absolute position measurement, only certain AUV trajectories are observable. Previous work proved that a system is observable by analysis of the Fisher information matrix [26]. Others proved trajectories are observable except those that are straight line segments passing through the origin (i.e., the beacon) [27], [28]. Other developments include a belief space planning algorithm to optimize trajectories of a team of AUVs to enhance observability and thus make the navigation solutions from these intervehicle ranges more accurate [29].

With the success of using OWTT range measurements from a single beacon to constrain XY position error, multiple vehicle navigation algorithms are using OWTT intervehicle range measurements to further constrain error. The main challenge in using intervehicle ranges for position estimates is overconfidence in the solution. Prior work in this area includes development of an algorithm in which the broadcasting vehicles share their pose and covariance estimates. This information is then used in a filter on a receiving vehicle to ensure conservative covariance estimates by preventing the use of measurements from the same origin more than once [30]. Another approach is an algorithm that computes odometry factors from the transmitting vehicle to prevent overconfidence in the receiving vehicle's solution based on intervehicle range measurements [31].

2) IMU Navigation: IMUs most commonly contain three orthogonal accelerometers, gyroscopes, and magnetometers that, respectively, measure linear acceleration, angular rates, and magnetic field strength. Thus, IMUs serve as a navigation sensor to determine a vehicle's attitude as well as serve as an odometry input by integrating the linear accelerations to obtain velocity and position. While reductions in size, power consumption, and cost of MEMS IMUs are occurring, their higher sensor noise levels and inaccuracy make them insufficient for many navigation applications compared to other high-end INS. For example, compared to a commercial grade INS (that costs on the order of tens of thousands of dollars, power consumption on the order of tens of watts, exhibits a drift of 0.001–1°/h for a fiber optic gyroscope, and 0.001–1 mg of acceleration bias for a pendulum accelerometer), an MEMS IMU gyroscope drifts greater than 60°/h, and its accelerometer exhibits 0.01–1 mg of bias [32], but it only costs on the order of tens of dollars and consumes power on the order of tens of milliwatts.

Many methods and algorithms reduce the errors of MEMS IMUs to make them suitable for underwater vehicle navigation. One such method is assessing an IMU's error statistics and then determining how best to select an IMU for a particular application [33]. Other methods consist of an EKF to estimate attitude

in a quaternion representation with depth measurements for improving accuracy [34]. Further, double integration of IMU linear accelerations provide a measurement for odometry in a navigation solution. A fused Kalman filter consisting of the GPS as well as IMU linear accelerations showed acceptable accuracy of a remotely operated vehicle but only consisted of a trial run of 10 s [35]. Better results of IMU accelerations as an odometry input are provided by an online EKF that fused IMU sensor measurements and GPS speed-over-ground measurements on a terrain vehicle that resulted in a root-mean-square (RMS) error of 17.4 m over a distance traveled of approximately 8.75 km in 51 min [36]. Additionally, in simulation, a combined translational and attitude observer, that used an IMU for both attitude and odometry, fused with DVL speed measurements resulted in an RMS position error of 0.5 m over 250 s of mission time [37].

Due to higher noise levels, bias errors, and drift errors from the accelerometers and gyroscopes, the double integration of the linear accelerations can lead to quite large position errors over time [38]. Since bias errors are known to drift over time, continuously updating and subtracting this bias error from a measurement can improve performance. Three angular-rate-aided estimators [39] improved bias estimation over previous methods of the TWOSTEP [40] and the attitude-independent EKF [41]. Others have improved performance by using an EKF to estimate bias and scale factor errors for both accelerometers and gyroscopes after a calibration procedure [42]. Finally, a first-order Gauss–Markov (GM) process, used to model bias estimation in a Kalman filter, showed convergence within 60 s for the gyroscopes and within 1 s for the accelerometers [43].

B. Contribution

This paper builds upon the research in single-beacon OWTT acoustic navigation and MEMS IMUs for measurements to determine AUV odometry and attitude. Using the high sample rate of IMU measurements coupled with a vehicle’s dynamic model velocity (based on propeller turn count) for speed measurements, this paper proposes an EKF, including accelerometer bias estimation and a coupled range filter (referred to herein as the IMU EKF), that produces position errors comparable to current standard navigation solutions. The main advantage to this approach is that a common inertial navigation strapdown sensor suite, notably a DVL, is not required; thus reducing size and cost and removing the operational area restriction of where DVL bottom lock is available—typically 30–300 m from the seafloor. Additionally, this paper shows that a coupled range filter is necessary to ensure that unreliable range measurements (due to environment variability, poor beacon state estimation, or hardware defects) are not processed by the IMU EKF. Field data from three different controlled-environment experiments in local waters and one open ocean experiment are presented proving this concept with a comparison of different navigation solutions.

This paper builds on the results from a previous work [21]. In that paper, we discussed a basic derivation of the IMU EKF navigation solution including the derivation of a complementary filter for estimating attitude used in this paper. Additionally, we

reported the initial field tests of implementing this method with results of average position error on the order of tens of meters with distances traveled of approximately 2 km. In this paper, we build on these results and contribute the following:

- 1) a theoretical derivation of the navigation solution model incorporating an EKF with acceleration bias estimation;
- 2) addition of a coupled range filter to the IMU EKF with theoretical derivation and experimental analysis;
- 3) analysis on navigation accuracy based on the effect of bias estimation and the number of transmitting beacons;
- 4) new field results with a Bluefin Robotics SandShark, Quincy, MA, USA, micro-AUV (μ AUV) and Iver2 AUVs in controlled local water environments as well as an open ocean experiment.

II. NAVIGATION MODEL

The Kalman filter [44] is a seminal state estimator used in many navigation solutions. Its wide use and applicability in this field are the reasons for choosing the EKF [45], a nonlinear variant of the Kalman filter, to serve as the state estimator in this paper.

The Kalman filter estimates a state by propagating a linear system’s state perturbed by Gaussian white noise and infers updates to the state by related measurements also perturbed by Gaussian white noise [46] as seen in the following equations:

$$\dot{\mathbf{x}}(t) = \mathbf{Ax}(t) + \mathbf{Dw}(t) \quad (1)$$

and

$$\mathbf{z}(t) = \mathbf{Hx}(t) + \mathbf{v}(t). \quad (2)$$

In (1) and (2), $\mathbf{x}(t)$ is the system’s state vector, \mathbf{A} is the system transition matrix, \mathbf{D} is the noise coefficient matrix, $\mathbf{z}(t)$ is the measurement, and \mathbf{H} is the state-to-measurement mapping matrix. The system process noise $\mathbf{w}(t)$ and measurement noise $\mathbf{v}(t)$ are considered zero-mean Gaussian white noise such that

$$\mathbf{w}(t) \sim \mathcal{N}(0, \mathbf{Q}_t), \quad \mathbf{v}(t) \sim \mathcal{N}(0, \mathbf{R})$$

where \mathbf{Q}_t is defined as the process-noise variance matrix and \mathbf{R} is the measurement noise variance matrix.

An overview block diagram of this IMU EKF implementation on the AUVs is displayed in Fig. 1. This block diagram shows all the different measurements and processes that are incorporated in this navigation model, which builds upon the navigation model presented in the previous work [21].

A. Plant Model

Since the OWTT range measurements are nonlinear, the Kalman filter variant used is an EKF, in which the nonlinear processes and/or measurements are linearized by a first-order Taylor series expansion and evaluated at the state’s value for that time step.

The vehicle’s state vector \mathbf{x}_v is defined as follows:

$$\mathbf{x}_v = [x, y, u, v, a_x, a_y, b_x, b_y]^T \quad (3)$$

where each $\{x, y\}$ pair is the vehicle’s XY position in the world frame (i.e., positive x is east, positive y is north, and positive z

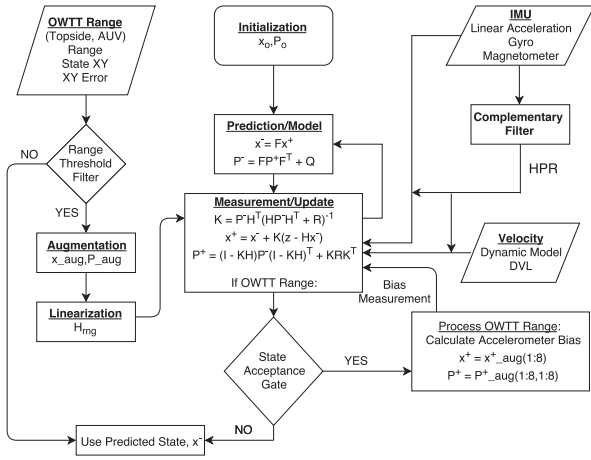


Fig. 1. Block diagram for the IMU EKF with a coupled range filter. This block diagram shows the start (rounded box), the processes (square), the input measurements (trapezoid), and the decision points by the coupled range filter (diamond).

is up), each $\{u, v\}$ pair is the vehicle's XY velocities in the world frame, and each $\{a_x, a_y\}$ pair is the vehicle's XY linear accelerations in the world frame. The $\{b_x, b_y\}$ elements are the respective XY acceleration bias terms in the world frame. Since attitude and depth are adequately instrumented, the z -dimensional parameters can be accurately measured and estimated. Thus, the 3-D OWTT range is projected into the horizontal plane, and only the XY position, velocity, acceleration, and biases are estimated.

The system model used for this EKF is a continuous Wiener process constant acceleration model [47] combined with an accelerometer bias model, and this model is used for the same reasons discussed in the prior results [21]. The system transition matrix \mathbf{A} and the noise coefficient vector \mathbf{D} from (1) are defined as follows:

$$\mathbf{A} = \begin{bmatrix} 0 & 0 & 1 & 0 & 0 & 0 & 0 & 0 \\ 0 & 0 & 0 & 1 & 0 & 0 & 0 & 0 \\ 0 & 0 & 0 & 0 & 1 & 0 & -1 & 0 \\ 0 & 0 & 0 & 0 & 0 & 1 & 0 & -1 \\ 0 & 0 & 0 & 0 & 0 & 0 & 0 & 0 \\ 0 & 0 & 0 & 0 & 0 & 0 & 0 & 0 \\ 0 & 0 & 0 & 0 & 0 & 0 & 0 & 0 \\ 0 & 0 & 0 & 0 & 0 & 0 & 0 & 0 \end{bmatrix} \quad (4)$$

and

$$\mathbf{D} = [0 \ 0 \ 0 \ 0 \ 1 \ 1 \ 0 \ 0]^T. \quad (5)$$

A first-order GM process is used to model the accelerometer bias as a random process. This model captures the slowly time-varying accelerometer bias because of its bounded uncertainty characteristic [43], [48], [49]. In discrete time, the bias \mathbf{b} is written as follows:

$$\mathbf{b}_k = e^{-\frac{dt}{T_c}} \mathbf{b}_{k-1} + \mathbf{w}_{b,k} \quad (6)$$

where dt is the sampling period, T_c is the correlation time constant, and \mathbf{w}_b is zero-mean bias process white noise with variance $\sigma_{w,b}^2$ with a tunable parameter σ_b^2 is given as follows:

$$\sigma_{w,b}^2 = \sigma_b^2 (1 - e^{-\frac{2dt}{T_c}}). \quad (7)$$

After a normal discretization of the state-transition matrix \mathbf{A} , the discrete-time GM process model in (6) for the bias terms are substituted in the appropriate elements of the discrete system transition matrix \mathbf{F} resulting in

$$\mathbf{F} = e^{\mathbf{A} dt}$$

$$= \begin{bmatrix} 1 & 0 & dt & 0 & \frac{1}{2}dt^2 & 0 & -\frac{1}{2}dt^2 & 0 \\ 0 & 1 & 0 & dt & 0 & \frac{1}{2}dt^2 & 0 & -\frac{1}{2}dt^2 \\ 0 & 0 & 1 & 0 & dt & 0 & -dt & 0 \\ 0 & 0 & 0 & 1 & 0 & dt & 0 & -dt \\ 0 & 0 & 0 & 0 & 1 & 0 & 0 & 0 \\ 0 & 0 & 0 & 0 & 0 & 1 & 0 & 0 \\ 0 & 0 & 0 & 0 & 0 & 0 & e^{-\frac{dt}{T_c}} & 0 \\ 0 & 0 & 0 & 0 & 0 & 0 & 0 & e^{-\frac{dt}{T_c}} \end{bmatrix}. \quad (8)$$

To derive the discrete-time process noise matrix \mathbf{Q} , the discrete-time process noise $\mathbf{v}(k)$ is determined as follows [47]:

$$\mathbf{v}(k) = \int_0^{dt} e^{\mathbf{A}(dt-\tau)} \mathbf{D} w(kdt + \tau) d\tau. \quad (9)$$

Initially, for the derivation, the transition matrix \mathbf{A} and the noise coefficient vector \mathbf{D} are based on the 2-D constant acceleration model only—i.e., this matrix and this vector do not contain the acceleration bias terms. Hence, their dimensions are 6×6 and 6×1 , respectively. The following discrete-time plant process noise covariance matrix \mathbf{Q} with gain parameter \tilde{q} is then derived:

$$\mathbf{Q} = E[\mathbf{v}(k)\mathbf{v}(k)^T] = \int_0^{dt} \begin{bmatrix} \frac{1}{2}(dt-\tau)^2 \\ \frac{1}{2}(dt-\tau)^2 \\ dt-\tau \\ dt-\tau \\ 1 \\ 1 \end{bmatrix} \times \begin{bmatrix} \frac{1}{2}(dt-\tau)^2 & \frac{1}{2}(dt-\tau)^2 & dt-\tau & dt-\tau & 1 & 1 \end{bmatrix} \tilde{q} d\tau. \quad (10)$$

To include the acceleration bias terms, \mathbf{Q} [defined in (10)] is expanded from 6×6 to 8×8 to include the discrete-time GM noise variance $\sigma_{w,b}^2$, and assuming that position, velocity, and acceleration in the different x and y dimensions are not correlated, and bias is not correlated with any other parameter, \mathbf{Q} reduces to the following:

$$\mathbf{Q} = \tilde{q} \begin{bmatrix} \frac{1}{20}dt^5 & 0 & \frac{1}{8}dt^4 & 0 & \frac{1}{6}dt^3 & 0 & 0 & 0 \\ 0 & \frac{1}{20}dt^4 & 0 & \frac{1}{8}dt^4 & 0 & \frac{1}{6}dt^3 & 0 & 0 \\ \frac{1}{8}dt^4 & 0 & \frac{1}{6}dt^3 & 0 & \frac{1}{2}dt^2 & 0 & 0 & 0 \\ 0 & \frac{1}{8}dt^4 & 0 & \frac{1}{6}dt^3 & 0 & \frac{1}{2}dt^2 & 0 & 0 \\ \frac{1}{6}dt^3 & 0 & \frac{1}{2}dt^2 & 0 & dt & 0 & 0 & 0 \\ 0 & \frac{1}{6}dt^3 & 0 & \frac{1}{2}dt^2 & 0 & dt & 0 & 0 \\ 0 & 0 & 0 & 0 & 0 & 0 & \sigma_{w,b}^2 & 0 \\ 0 & 0 & 0 & 0 & 0 & 0 & 0 & \sigma_{w,b}^2 \end{bmatrix}. \quad (11)$$

B. Observation Models

The velocity, linear acceleration, and bias observation measurements are linear. Conversely, the OWTT range measurement is nonlinear; thus the measurement (2) becomes

$$\mathbf{z}(t) = h(\mathbf{x}(t)) + \mathbf{v}(t) \quad (12)$$

where $h(\mathbf{x}(t))$ is the nonlinear range function, discussed in more detail in Section II-B1. In discrete time, the measurement model becomes

$$\mathbf{z}_k = \mathbf{H}_k \mathbf{x}_{\mathbf{v}_k} + \tilde{\mathbf{v}}_k. \quad (13)$$

The measurement variable \mathbf{z}_k represents the type of measurement (i.e., velocity, linear acceleration, bias observation, or OWTT range) for a particular time step k . As shown in (13), the observation noise $\tilde{\mathbf{v}}_k$ is zero-mean Gaussian white noise such that

$$\tilde{\mathbf{v}}_k \sim \mathcal{N}(O, \mathbf{R}_k). \quad (14)$$

For the measurement variance noise matrix \mathbf{R}_k , the matrix is diagonal with the respective measurement (dynamic model velocity, acceleration, bias, or range) variance values

$$\mathbf{R}_{\text{vel}} = \begin{bmatrix} \sigma_{\text{vel}}^2 & 0 \\ 0 & \sigma_{\text{vel}}^2 \end{bmatrix} \quad (15)$$

$$\mathbf{R}_{\text{acc}} = \begin{bmatrix} \sigma_{\text{acc}_x}^2 & 0 \\ 0 & \sigma_{\text{acc}_y}^2 \end{bmatrix} \quad (16)$$

$$\mathbf{R}_{\text{bias}} = \begin{bmatrix} \sigma_{\text{bias}}^2 & 0 \\ 0 & \sigma_{\text{bias}}^2 \end{bmatrix} \quad (17)$$

and

$$R_{\text{rng}} = [\sigma_{\text{rng}}^2]. \quad (18)$$

Since the vehicle's DVL and IMUs are adequately defined and calibrated, modeling their noise characteristics as zero-mean Gaussian noise is acceptable. However, acoustic range measurements are often not characteristic of zero-mean Gaussian noise because of such factors as multipath propagation and varying sound-velocity profiles. To minimize the error in the filter's estimate using the zero-mean Gaussian observation noise assumption, large standard deviation values (see Tables II and IV) were used as the σ_{rng} values in the IMU EKF. This method was proven successful in a previous work [18].

1) Range Measurement and Augmentation: To process an OWTT range measurement, the vehicle's state vector and covariance matrix must be augmented with the transmitting beacon's position and time information. This process resembles the process presented in the previous work [21] and is summarized here for ease of reference.

The vehicle's state vector is augmented with the transmitting beacon's position $[x_b, y_b]$ such that

$$\mathbf{x}_{\text{aug}} = [x, y, u, v, a_x, a_y, b_x, b_y, x_b, y_b]^T \quad (19)$$

Similar to the naively distributed EKF (NEKF) [15], the \mathbf{P} matrix is augmented with the transmitting beacon's position uncertainty

values in the following manner:

$$\mathbf{P}_{\text{aug}} = \begin{bmatrix} \mathbf{P}_v & \mathbf{0} & \mathbf{0} \\ \mathbf{0} & \sigma_{\text{beacon}}^2 & 0 \\ \mathbf{0} & 0 & \sigma_{\text{beacon}}^2 \end{bmatrix} \quad (20)$$

where \mathbf{P}_v is the vehicle's predicted 8×8 covariance matrix at time k of the range measurement. Different from the NEKF, σ_{beacon}^2 is the sum of the X and Y position variances of the transmitting beacon; thus making this method more conservative than the true NEKF method, which uses the individual X and Y position variance values. Additionally, similar to the NEKF, correlation between the submerged platforms is prevented since the platforms receive range measurements from a GPS-localized beacon. Using the sum of the X and Y position variances and receiving ranges from a GPS-localized beacon aid in minimizing the potential for overconfident solutions. For the surface beacon, the GPS uncertainty is transmitted as a single value, which is used as the value of σ_{beacon} .

The state-to-measurement mapping matrix for an acoustic range \mathbf{H}_{rng} is determined following the augmentation process. The OWTT range model is based upon the model presented in previous field experiments [18] such that the range between the beacon at time of launch (TOL) and the vehicle at time of arrival (TOA) is modeled in vector form with a time-invariant noise v_{rng} as the following:

$$z_{\text{rng}} = (\mathbf{x}^T \mathbf{M}^T \mathbf{M} \mathbf{x})^{1/2} + v_{\text{rng}} \quad (21)$$

where

$$\mathbf{M} = [\mathbf{J}_v \ -\mathbf{J}_b] \quad v_{\text{rng}} \sim \mathcal{N}(0, R_{\text{rng}}) \quad (22)$$

$$\mathbf{J}_v = [\mathbf{I}_{2 \times 2} \ \mathbf{0}_{2 \times 6}] \quad (23)$$

and

$$\mathbf{J}_b = [\mathbf{I}_{2 \times 2}]. \quad (24)$$

\mathbf{J}_v and \mathbf{J}_b are defined to capture the pose information of the vehicle and the beacon at TOA and TOL, respectively. With the nonlinearity in the range (21), a Jacobian matrix of this equation, evaluated at the vehicle's augmented predicted state becomes

$$\mathbf{H}_{\text{rng}_k} = \frac{\partial z_{\text{rng}}}{\partial \mathbf{x}} \Big|_{\mathbf{x}=\hat{\mathbf{x}}_{\text{aug}_k}} = [(\hat{\mathbf{x}}_{\text{aug}_k}^-)^T (\mathbf{M}^T)(\mathbf{M})(\hat{\mathbf{x}}_{\text{aug}_k}^-)]^{-1/2} \times (\hat{\mathbf{x}}_{\text{aug}_k}^-)^T (\mathbf{M}^T)(\mathbf{M}). \quad (25)$$

With each \mathbf{H}_{rng} matrix, the Kalman filter measurement update equations (noted in the "Measurement/Update" block in Fig. 1) are processed, and the vehicle's state and covariance matrix is updated with this OWTT range measurement.

C. Coupled Range Filter

The IMU EKF is coupled with a range filter to prevent processing a range measurement that results in an unstable state estimate. A faulty range can result from poor clock synchronization between the transmitter and the receiver or from acoustic environmental variability. A small amount of drift on either clock can change the TOL or TOA of the acoustic packet and

Algorithm 1: IMU EKF Coupled Range Filter Applied to OWTT Range Measurements.

```

1: while Processing IMU EKF do
2:   if Receive OWTT Range measurement then
3:     Process maximum operating range filter:
4:     if OWTT Range < maximum operating range then
5:       Process range measurement in EKF
       measurement update step
6:     else
7:       Use predicted state.
8:     end if
9:     Process state-acceptance gate by (26)
10:    if Updated state passes acceptance gate then
11:      Use updated state and continue processing IMU
         EKF
12:    else
13:      Use predicted state.
14:    end if
15:  end if
16: end while

```

thereby change the range calculation. Additionally, acoustic environments that contain multipath propagation or reflection can result in incorrect TOF measurements of the slant range between the transmitting beacon and receiving vehicle; thus making the OWTT range measurement inaccurate.

When processing a range measurement, the subsequent updated state estimate can be unreliable if the transmitting beacon's state, as encoded in the acoustic packet, is inaccurate. The Jacobian OWTT range state-to-measurement mapping matrix \mathbf{H}_{rng} [see (25)] uses the transmitting beacon's state in its calculation, and this matrix is then used to update the receiving vehicle's state with the innovation. Therefore, any inaccuracy in the transmitting beacon's state estimate can easily contribute to an error in the receiving vehicle's state estimate as soon as the OWTT range is processed. To address these issues, the coupled range filter in the IMU EKF uses two different processes to prevent the IMU EKF from processing a faulty range measurement. These two processes are a maximum operating range filter and a state-acceptance gate, both summarized in Algorithm 1.

The first decision point of the coupled range filter is the maximum operating range filter, which prevents the IMU EKF from processing the measurement update equations on a faulty range. Simply, if the OWTT range is greater than the set maximum range value, the range is discarded and the measurement update equations are not processed. The maximum operating range value can be determined in a variety of methods. Examples include geographic constraints or known acoustic range limitations based on environment or equipment.

After the vehicle's updated state is determined, a state-acceptance gate (analogous to a velocity filter) is applied to prevent processing a receiving vehicle's updated state estimate due to an inaccurate beacon's state estimate. The IMU EKF tracks its previous state estimated position and time from the last OWTT range measurement from any beacon. After determining

the updated state, the IMU EKF calculates a distance from the vehicle's state position at the time of the last range measurement to the current vehicle's updated state position. This distance is then divided by the time since the last OWTT range update. This calculation results in a speed, which is then compared to a predetermined speed value. If the calculated speed is less than this predetermined value, the updated state is processed and an acceleration bias measurement is determined. If the calculated speed is greater than the predetermined speed value, the updated state estimate is disregarded and the vehicle's predicted state is propagated forward. Equations (26) and (27) show the speed calculation, where x and y are the vehicle's estimated position coordinates in the world frame and k and t are the current time and last range update time, respectively

$$\frac{\sqrt{(x_k - x_t)^2 + (y_k - y_t)^2}}{\Delta t} < \text{predetermined speed value} \quad (26)$$

$$\Delta t = k - t. \quad (27)$$

This predetermined speed value used can be determined by the vehicle's maximum rated speed or the mission's maximum commanded speed with a deviation. For example, if the mission's commanded speed is 1.3 m/s and the vehicle is using its DVL for speed measurements, the speed value for the state-acceptance gate could be set to 1.5 m/s, which provides a 15% deviation to allow for any variability in the DVL measurements.

III. EXPERIMENTAL CONFIGURATION

A. Vehicles

OceanServer Technology, Inc., Fall River, MA, USA, Iver2 vehicles and a Bluefin Robotics SandShark μ AUV were used during the field trials for this research. Details of these three platforms are discussed further in Sections III-A1 and III-A2.

1) *OceanServer Technology, Inc., Iver2 AUV*: Two Iver2 AUVs [50], Iver-106 and Iver-136, were deployed for three field trials during the course of this work. These two vehicles on board the *R/V Shana Rae* for the “Satellites to the Ocean Floor” research project [8] along with their configuration layout are featured in Fig. 2. Details of their configuration are discussed in the previous work [21], and this configuration remained the same for all additional field experiments discussed in this paper unless explicitly described otherwise.

Throughout the field trials, these vehicles used a dynamic model velocity as a speed measurement for their navigation solutions. To determine these values, a series of speed trials were conducted to determine the correlation between vehicle speed-over-ground and propeller motor speed. These results were used to build a motor-speed table, which was used on board the vehicle as well as the MATLAB implementations of the IMU EKF (see Section III-C).

2) *Bluefin Robotics SandShark μ AUV*: The Bluefin Robotics SandShark used in these field experiments was a small low-cost μ AUV that has been configured with a payload suitable for acoustic navigation [52]. Specifically, this vehicle was equipped with a 9-DOF MEMS IMU collocated on an Android phone

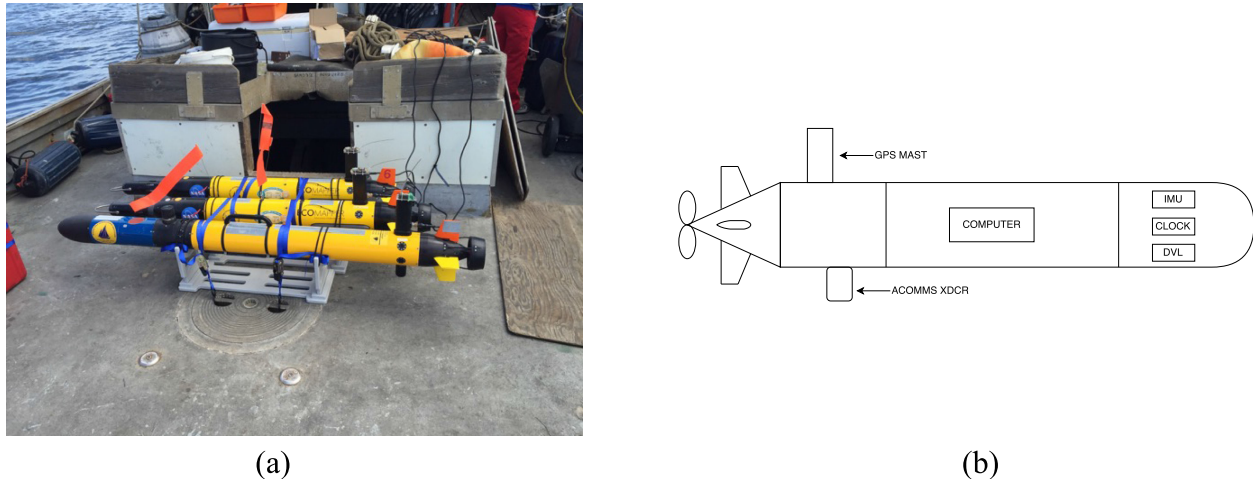


Fig. 2. (a) OceanServer Iver2 AUVs on board the *R/V Shana Rae*. Front to back: Iver-136, Iver-107, Iver-106, Iver-106, and Iver-106 were used in the field experiments described in this paper. Photo courtesy of Dr. D. Frattoni during the KISS field project in 2016 [20], [51]. (b) Iver2 AUV system's configuration layout: displays the main components and sensors necessary for the IMU EKF navigation method [20].



Fig. 3. Bluefin Robotics SandShark μ AUV. (a) SandShark μ AUV before field trials conducted on the Charles River in Cambridge, MA, USA. (b) Nose cone removed to display the acoustic tetrahedral hydrophone array. Pictures from proof of concept trials of the acoustic navigation payload [52].

device computer board, an altimeter, a depth sensor, an acoustic micromodem, and a GPS receiver. A unique payload configuration for this particular SandShark was the tetrahedral hydrophone array used for its acoustic communications (ACOMMS), as shown in Fig. 3.

The Sandshark also used a dynamic model velocity as a speed measurement for all of its navigation solutions. Like the Iver2 vehicles, the SandShark's dynamic model velocity directly correlated to its propeller motor speed. However, instead of conducting separate speed trials to determine this correlation, values given by the manufacturer were used in these experiments.

B. Acoustic Communications (ACOMMS)

1) *Iver2 AUVs Communications:* Both the topside node and the submerged nodes for the Iver2 vehicles operated the same ACOMMS software on their own Ubuntu Linux computers. This ACOMMS network is similar to the one used in previous successful field results [16], and the configuration used in this research is identical to the one presented in the prior work [21]. As discussed in the previous paper, the time synchronization error between the nodes is critical for the accuracy of the OWTT range measurements. The drift between the node's NTP servers was observed to be less than 1 ms and did not drift beyond this error throughout the experiments. Thus, for an assumed sound

velocity of 1500 m/s, the resulting range error was less than 1.5 m.

2) *SandShark μ AUV ACOMMS:* The original intent of this SandShark configuration with the tetrahedral array was for inverted USBL OWTT navigation [53], [54]. However, for the purpose of this work, this platform used the tetrahedral array for OWTT range measurements. Each of the four elements of the acoustic array processed a range estimate by a matched filtering process, and these resulting ranges were the raw measurements sent to the IMU EKF. Because each element processed a range, the median of these four ranges was used as the range measurement in the IMU EKF. The SandShark used a Microsemi, Aliso Viejo, CA, USA, SA.45 CSAC for precision time keeping and synchronization [23], [55].

A topside acoustic source was lowered dockside in the Charles River during these experiments. This source transducer was synchronized with a GPS pulse per second (PPS) signal and transmitted its GPS location and TOL, which was then decoded by the SandShark. During these experiments, the topside source transmitted a frequency of 1 Hz.

C. IMU EKF Implementation

During the field experiments for this research, the lightweight communications and marshalling [56] system for the Iver2 vehicles and a similar system on the SandShark vehicle recorded data from all the various sensors. Using MATLAB, the IMU EKF navigation method (described in detail in Section II) processed the time-sequential data from the field experiments. The results from this implementation of the IMU EKF in MATLAB are those used for analysis in this paper.

IV. LOCAL WATERS FIELD RESULTS

A series of trials were conducted to validate the IMU EKF navigation solution. These trials consisted of different platforms, distinct acoustic environments, and diverse mission trajectories and configurations to present performance summaries with experimental diversity. The first three experiments were conducted in controlled environments of local waters, and the last

TABLE I
NAVIGATION SOLUTION DESCRIPTION SUMMARY

Solution Type	Description	Inputs	Field Trial Location
IMU EKF	Constant acceleration model, Includes bias estimation, Includes coupled range filter	Linear accelerations, Dynamic Model Velocity or DVL, TOF range measurements	Ashumet Pond 2016 Charles River 2016 Ashumet Pond 2017 Monterey Bay 2016
DR EKF	Constant acceleration model, No bias estimation	Linear accelerations, Dynamic Model Velocity or DVL	Ashumet Pond 2016 Charles River 2016 Ashumet Pond 2017 Monterey Bay 2016
CL EKF (Iver2)	Constant velocity model, No range filtering	Dynamic Model Velocity or DVL, TOF range measurements, GPS (Ashumet Pond 2017 only)	Ashumet Pond 2016 Ashumet Pond 2017 Monterey Bay 2016
SS CL (SandShark)	Model-velocity aided dead-reckoned,	Model-velocity, GPS	Charles River 2016

experiment provides results from an open ocean environment (discussed in Section V).

The first analysis of the October 2016 Iver2 field experiments proves the effectiveness of the bias estimation in the IMU EKF and the use of multiple transmitting OWTT beacons. The second field experiment consisting of the SandShark μ AUV on the Charles River offers a distinct platform and mission configuration and demonstrates the capability of the coupled range filter. The last experiment conducted on the Iver2 vehicles in April 2017 in Ashumet Pond confirms the capability of the coupled range filter in a multivehicle trajectory that is indicative of current real-world AUV missions. Finally, the open water experiment was conducted with one of the Iver2 vehicles in Monterey Bay, CA, USA, providing performance results of this navigation method in open ocean currents. Details of these experiments and the associated analyses are explained in Sections IV-A–IV-C.

A variety of navigation solutions are presented for comparison in all of the following analyses: IMU EKF, DR EKF, closed-loop EKF (CL EKF), and the SandShark CL navigation solution (SS CL). Details of these solutions are discussed in each individual experiment section, and Table I provides a summarized description of their inputs and the field trial locations where they were utilized. The CL solutions for the Iver2 vehicles and the SandShark were the navigation solutions used on board the vehicles during the conduct of the field trials. Optimization of CL solutions was not analyzed for the purpose of this paper.

A. Ashumet Pond 2016

The analysis of this field data builds upon our prior work [21]. The dynamic model velocity aided IMU EKF produced an average error of 10.26 m for Iver-106 and 12.95 m for Iver-136 over distances traveled of 1.73 and 1.91 km, respectively. The analysis herein investigates the effect on the navigation accuracy of the bias estimation and the number of beacons serving to provide the OWTT range measurements. For reference, the IMU EKF parameter values for the Iver2 vehicles are noted in Table II.

In postprocessing, the IMU EKF solution was renavigated with the different combinations of bias estimation and num-

TABLE II
VEHICLE IMU EKF PARAMETER VALUES. (a) IVER-106 IMU EKF.
(b) IVER-136 IMU EKF

Parameter	Value	Parameter	Value
dt	0.037 s	dt	0.039 s
\tilde{q}	1.0	\tilde{q}	1.0
σ_b	1.0 m/s ²	σ_b	1.0 m/s ²
σ_{vel}	1.0 m/s	σ_{vel}	1.0 m/s
σ_{acc_x}	0.945 mg	σ_{acc_x}	0.631 mg
σ_{acc_y}	0.976 mg	σ_{acc_y}	0.682 mg
σ_{bias}	1.0 m/s ²	σ_{bias}	1.0 m/s ²
σ_{rng}	10 m	σ_{rng}	10 m
T_{c_x}	100 s	T_{c_x}	100 s
T_{c_y}	500 s	T_{c_y}	500 s

(a) (b)

bers of beacons available for OWTT range measurements. The dynamic model velocity was used for the speed measurement in all of these scenarios. All the parameters given in Table II remained the same for these renavigated solutions except the process noise gain \tilde{q} , which is equal to 100 instead of 1.0 for both Iver-106 and Iver-136 for those scenarios consisting either of a single beacon or the absence of bias estimation. A summary of the average error results for both Iver-106 and Iver-136 is presented in Table III. In this table, “Y” indicates that the bias estimator or both beacons were used in the solution. Conversely, “N” indicates that the bias estimator was not used or only the topside beacon was used for the OWTT range measurements.

As the results in Table III show that both the bias estimator and the use of the other vehicle serving as a beacon aided in reducing the overall position error by significant margins. For Iver-106, with both beacons present, the bias estimator included in the IMU EKF improved the solution by 23.1%. Without the bias estimator, including the other vehicle as beacon improved

TABLE III
IMU EKF BEACON AND BIAS ANALYSIS RESULTS SUMMARY. (a) IVER-106 IMU EKF. (b) IVER-136 IMU EKF

All Beacons	Bias Estimation	Average Error
Y	Y	10.26 m
Y	N	13.34 m
N	Y	14.04 m
N	N	13.86 m

All Beacons	Bias Estimation	Average Error
Y	Y	12.95 m
Y	N	17.82 m
N	Y	14.26 m
N	N	17.09 m

(a)

(b)

the solution by only 3.8%, which is considered insignificant and within the uncertainty of the experiment. With only the surface beacon present, the bias estimator did not improve the average error, but the average error increase was less than 1 m, which is considered minimal. However, the largest improvement of 26.9% was made by including the additional beacon when bias estimation was present.

For Iver-136, similar results were observed. Bias estimation improved the solution by 27.3% with both beacons present. Unlike Iver-106, without bias estimation present and with the additional beacon, performance decreased, but the average error increased by less than 1 m and is considered within the experimental uncertainty. Additionally, unlike Iver-106, with a single beacon, bias estimation lowered the error by 16.6%. Nonetheless, similar to Iver-106, the addition of another beacon improved the solution by 9.2% with bias estimation present. Overall, the additional beacon had less of an influence on solution improvement than did the presence of bias estimation, but the combination of the two contributed an overall accuracy improvement. Because of these results, analysis of the subsequent field trials all include bias estimation and, when available, multiple beacons.

B. Charles River 2016

A Bluefin Robotics, Inc., SandShark μ AUV was deployed for a field trial on the Charles River on October 17, 2016 for the Massachusetts Institute of Technology (MIT) Laboratory for Acoustic Marine Sensing Systems, Cambridge, MA, USA. The main purpose for using this field data was to assess the accuracy of the IMU EKF on a different platform, acoustic environment, and mission trajectory. Additionally, this experiment demonstrates the importance and necessity of the coupled range filter to the IMU EKF to preserve solution accuracy.

The vehicle's CL navigation solution used during this field trial was a dynamic model velocity based DR solution (referred to as SS CL); it used GPS measurements but did not incorporate any OWTT range measurements. Both the IMU EKF and DR EKF implementations on this field data used a dynamic model velocity for speed measurements, but neither of these solutions used the GPS. The IMU EKF did process the OWTT measurements from the topside beacon, but the DR EKF did not process these measurements nor did it incorporate any bias estimation.

The IMU EKF implemented herein on the SandShark is the same as presented in Section IV-A for the Iver2 AUVs except that this IMU EKF processed a median range from the four ranges acquired by the tetrahedral array, as described in

TABLE IV
SANDSHARK IMU EKF PARAMETER VALUES

Parameter	Value
dt	0.015 s
σ_b	1.0 m/s ²
T_{c_x}	1000 s
T_{c_y}	1000 s
\tilde{q}	0.1
Max Operating Range	130 m
Max Speed	1.54 m/s
σ_{rng}	3.3 m
σ_{vel}	1.0 m/s
σ_{accel}	0.1 m/s ²
σ_{bias}	0.1 m/s ₂

Section III-B2. The parameter values for the SandShark IMU EKF are summarized in Table IV.

The SandShark μ AUV was deployed from a dock on the Charles River. The vehicle's navigation solution was initialized on the dock, and the vehicle was then hand carried to the water where it was immediately submerged for its mission. The vehicle followed a lawnmower pattern trajectory with a mission time of 15.85 min, a submerged commanded depth of 2 m, and a commanded speed of 1 m/s except when on the surface. The vehicle surfaced twice during the mission: once at approximately 9 min into the mission and then at mission completion. During both of these surfacing periods, the vehicle's commanded speed was 0 m/s and it processed GPS position fixes during both periods. The topside beacon transmitted acoustic packets at a frequency of 1 Hz and the vehicle experienced 28.50% acoustic packet loss over the course of its mission.

Due to the high frequency of range measurements from the topside beacon, the highly reflective acoustic environment of the Charles River, and the self-occlusion effect on the matched filtering process [54], numerous inaccurate ranges were observed by the tetrahedral array on the vehicle. The blue points in Fig. 4 indicate these erroneous raw ranges.

Without the coupled range filter, with the IMU EKF processing all the received raw OWTT ranges, the solution produced an unstable trajectory. Conversely, by incorporating the coupled

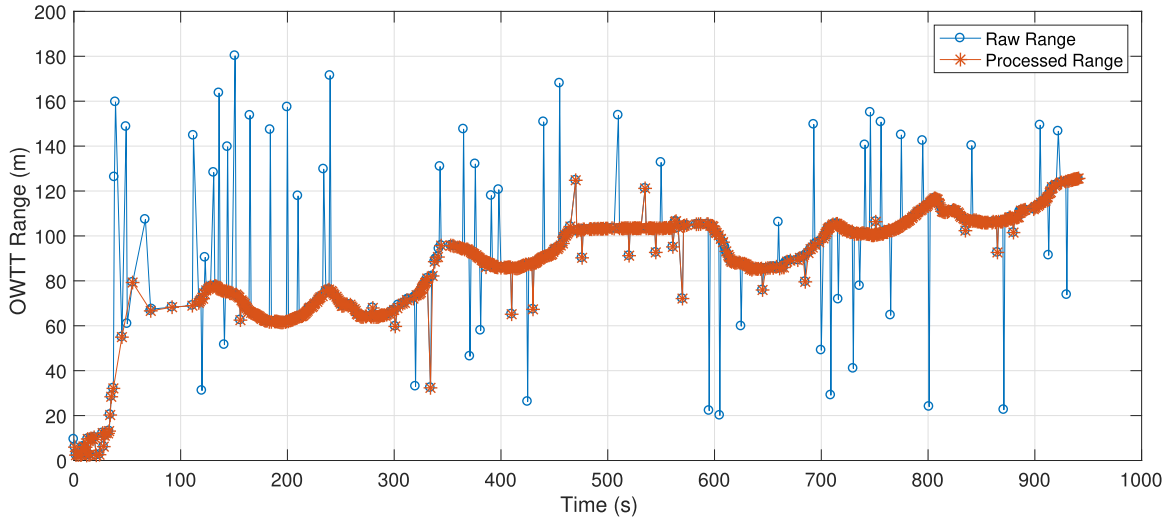


Fig. 4. SandShark-processed OWTT ranges. The raw OWTT ranges (blue) are plotted with the processed OWTT ranges (red) by the IMU EKF. These processed ranges result from passing the required conditions of the coupled range filter.

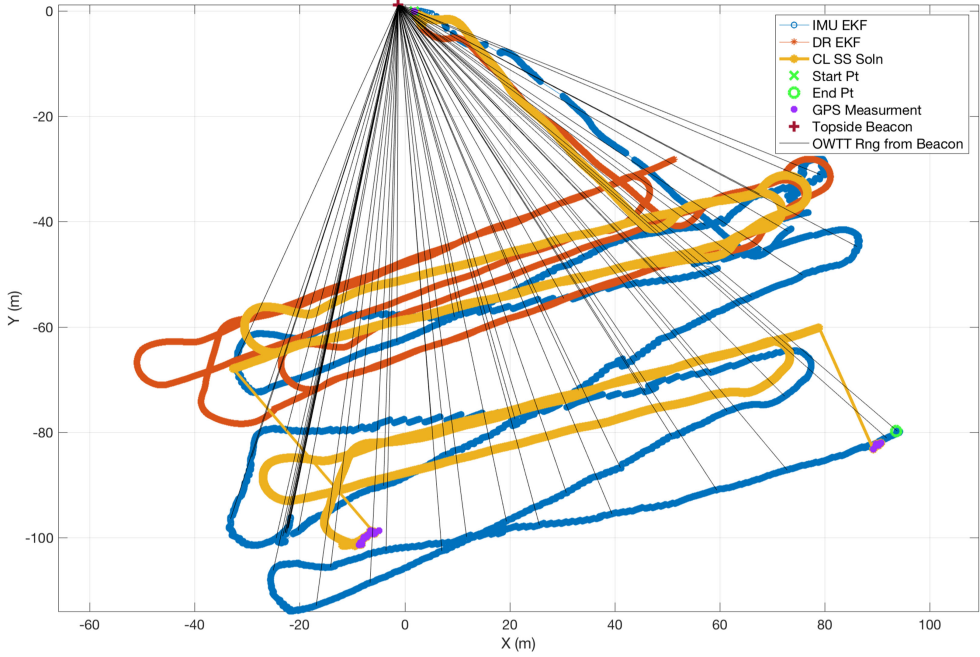


Fig. 5. SandShark EKF position summary: IMU EKF (blue), DR EKF (brown), and SS CL solution (gold). The black lines indicate the OWTT ranges from the stationary topside beacon to the vehicle's updated position. To prevent plot clutter, every tenth range processed by the IMU EKF is plotted.

range filter with the parameter values shown in Table IV, significant improvement was observed in the vehicle's XY trajectory. Of the total 686 OWTT raw ranges from the topside beacon, 26 ranges were removed by the max operating range filter and 62 ranges were removed by the state-acceptance gate. Fig. 4 shows the IMU EKF processed OWTT ranges against the received raw OWTT ranges. As this figure shows, the coupled range filter prevented a majority of the erroneous ranges from being processed by the IMU EKF.

By processing the OWTT ranges given by the coupled range filter, as presented in Fig. 4, a more stable trajectory resulted, as shown in Fig. 5, which shows the IMU EKF (blue), the DR EKF (red), and the CL SS (gold) navigation solutions. As illustrated,

the IMU EKF is the solution that most closely matches the GPS fixes (purple) when the vehicle surfaces at the mission's midpoint and endpoint.

The source of ground truth for this field data was the GPS position fixes during the two surfacing periods in the mission. Fig. 6 displays the time-series error of the three navigation solutions compared to the GPS position, and the IMU EKF exhibited an average error of 12.23 m, which was the smallest error of all three solutions for the SandShark. Average errors from GPS positions for the other solutions are summarized in Table V. To provide a more accurate comparison, points after the SS CL solution accepted GPS position fixes are removed from the error calculation for the average value shown in the table.

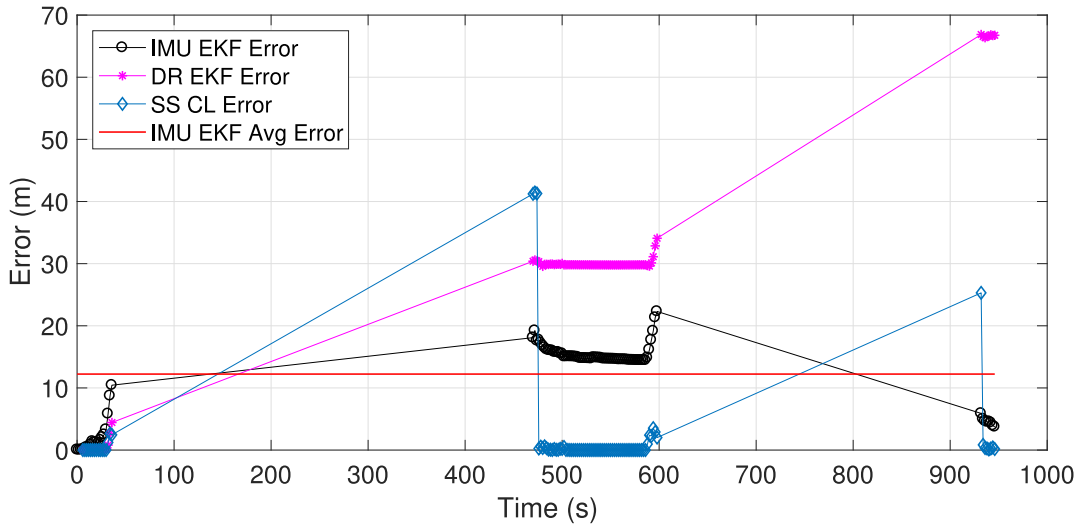


Fig. 6. SandShark performance summary. This plot displays the IMU EKF error (black), the DR EKF error (magenta), and the SS CL error (light blue) compared to the GPS locations at the time the vehicles surfaced during the mission. The average IMU EKF error (brown) is plotted for comparison.

TABLE V
SANDSHARK NAVIGATION PERFORMANCE SUMMARY

Parameter	Performance Result
Amount of Filtered Ranges	12.94 %
IMU EKF Average Error	12.22 m
DR EK Average Error	27.99 m
SS CL Average Error	37.32 m

C. Ashumet Pond 2017

A third field trial with the Iver2 AUVs was conducted on Ashumet Pond in April 2017 to assess the reliability of the IMU EKF with the coupled range filter in a multiple vehicle mission trajectory that resembled current real-world AUV applications of a lawnmower-type pattern with periodic surfacings. Thus, this experiment consisted of submerged legs that were longer in length and time than those of the previous trials. The periodic surfacing periods provided the truth positions from the GPS to determine position error for the navigation solutions.

These field trials used the same vehicles with identical configurations as discussed in the field results from October 2016 along with the same surface skiff to serve as the topside beacon. Additionally, the ACOMMS network between the vehicles and the topside beacon was identical to the experiment conducted in October 2016. Both Iver-106 and Iver-136 commenced their missions simultaneously, but the initial mission on Iver-106 unexpectedly ended, which necessitated troubleshooting on Iver-106 during the first 2000 s of the overall mission. Hence, in this analysis, the mission for Iver-106 started approximately 2000 s after Iver-136. However, during this troubleshooting window, Iver-106 did transmit several acoustic packets to Iver-136. These packets were received and processed by Iver-136, and those acoustic ranges are presented in this analysis.

This analysis presents three different navigation solutions: the IMU EKF, the CL EKF, and the DR EKF. For Iver-106, the CL EKF used its DVL for speed measurements as well as the GPS. However, because the vehicle's depth sensor did not properly zero when the vehicle surfaced, GPS fixes were not incorporated into the CL EKF starting at $t = 3313$ s. Iver-136, on the other hand, used a vehicle dynamic model velocity for its CL EKF's speed measurement and incorporated all GPS fixes throughout its mission. The DR EKF used the same data measurements as the IMU EKF but did not incorporate any of the OWTT ranges nor the bias estimation.

The CL EKF did not incorporate any additional filtering on the TOF range measurements, so it was susceptible to faulty ranges due to poor clock synchronization, acoustic environment, or poor position state estimates provided by the transmitting beacon. Fig. 7 shows the CL EKF trajectory summaries for both Iver-106 and Iver-136, and these plots clearly demonstrate how the absence of additional range filtering can adversely affect the accuracy of the navigation solution. In Sections IV-C1 and IV-C2, each vehicle is analyzed individually with a focus on the effectiveness of the coupled range filter to the IMU EKF's accuracy in a multivehicle navigation scenario.

1) *Iver-106 Performance:* In this analysis, the IMU EKF was implemented with both the vehicle's dynamic model velocity and its DVL as the speed measurement. Additionally, due to battery replacement of Iver-106, the previous calibration for the Pololu, Las Vegas, NV, USA, IMU magnetometer was inaccurate; thus the manufacturer MEMS compass provided the attitude measurements. Due to the incorporation of the coupled range filter and the manufacturer compass in this implementation, the velocity standard deviation σ_{vel} and the frequency of the IMU EKF dt for the IMU EKF required different values. The parameters given in Table II remained the same except those identified in Table VI.

As given in Table VI, the maximum speed value for the state-acceptance gate is different for the dynamic model velocity and DVL-aided IMU EKFs. Since the commanded speed for the

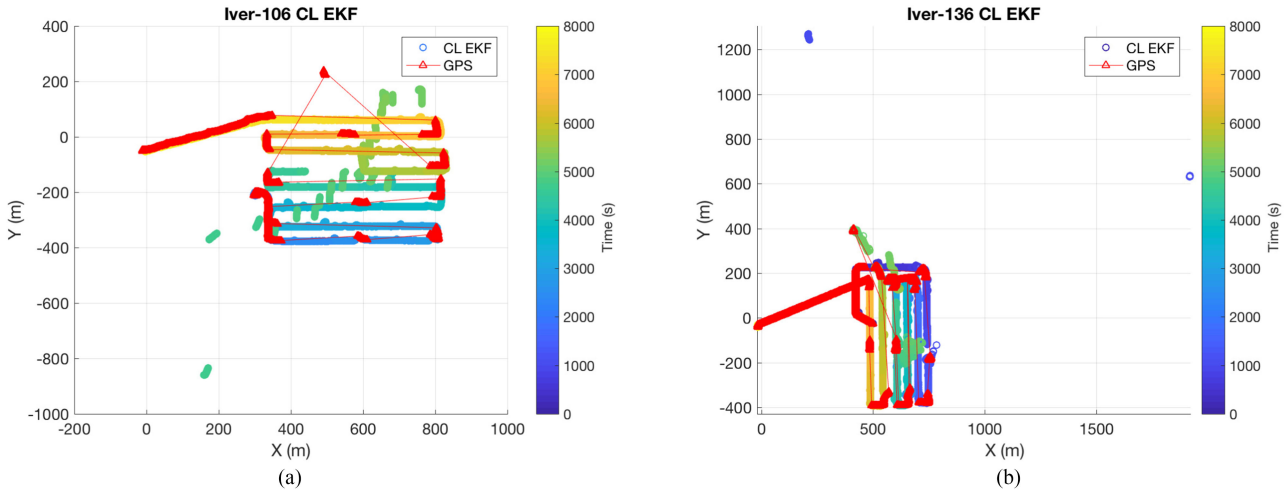


Fig. 7. Iver2 CL EKF trajectory summaries. (a) Iver-106 CL EKF trajectory summary and (b) Iver-136 CL EKF trajectory. Each plot shows a time color bar plot of the vehicle's estimated position along with its GPS position fixes (red) when the vehicle surfaced. The mission for Iver-106 commenced approximately 2000 s after Iver-136. During this time window, Iver-106 did pass several acoustic packets while troubleshooting was conducted to fix the unexpected behavior. These plots show the significant effect of not applying additional filtering on the TOF range measurements. Note the difference in scale between the two plots, which further demonstrates the adverse effect of a faulty range on the estimated position.

TABLE VI
IVER-106 IMU EKF PARAMETER VALUES. (a) MODEL VELOCITY AIDED.
(b) DVL AIDED

Parameter	Value
σ_{vel}	10.0 m/s
dt	0.085 s
Max Speed	1.29 m/s

(a)

Parameter	Value
σ_{vel}	5.0 m/s
dt	0.085 s
Max Speed	2.06 m/s

(b)

TABLE VII
IVER-136 IMU EKF PARAMETER VALUES. (a) MODEL VELOCITY AIDED.
(b) DVL AIDED

Parameter	Value
σ_{vel}	1.0 m/s
dt	0.042 s
Max Speed	1.54 m/s

(a)

Parameter	Value
σ_{vel}	1.0 m/s
dt	0.042 s
Max Speed	1.54 m/s

(b)

mission was 1.03 m/s, the maximum speed was set at 1.29 m/s providing a 25% conservative boundary for inaccurate dynamic model velocity speed measurements. For the DVL-aided IMU EKF, 2.06 m/s was used because the DVL provides a more accurate speed measurement with a higher variability, and 2.06 m/s is the maximum rated speed of the vehicle.

The trajectory summaries for the IMU EKF using both the vehicle dynamic model velocity and the DVL are shown in Fig. 8 and the error summaries are shown in Fig. 9. As the plots show, the IMU EKF tracks closely with the GPS measurements throughout the mission for both types of speed measurements. Both types of solutions are comparable in accuracy, but, as expected, the DVL-aided IMU EKF lowered the position uncertainty by a factor of approximately 2. As the plots show, especially in Fig. 8(b) with the direct comparison of the DVL-aided CL EKF, these two IMU EKF solutions do not exhibit the same erratic behavior of the CL EKF. Both solutions show true vehicle movement to the North as evident by the GPS fix at position (490, 225). With this more accurate trajectory, both of the IMU EKF errors are considerably less than the CL EKF error, especially at time $t = 5000$ s when the vehicle drove north.

Another representation summarizing the performance of the IMU EKF with the coupled range filter is a time-series plot of the individual X and Y position estimates for both the IMU EKF and CL EKF compared to the GPS fixes, as shown in Fig. 10. This plot displays the DVL-aided IMU EKF to provide

a better comparison with the DVL-aided CL EKF. As shown, the erroneous behavior from the CL EKF (red) from 4700 to 5200 s was replaced by a more constant trajectory exhibited by the IMU EKF (green) during the same time period without the eccentric position estimate jumps of approximately 800 m and 500 m at time $t = 4700$ and 5100 s, respectively. As previously noted on the depth sensor issue, the CL EKF did not incorporate GPS fixes after time $t = 3313$ s; thus this solution did not process the GPS fix at position (490, 225) $t = 5000$ s. However, the coupled range filter prevented the IMU EKF from processing the poor OWTT range measurements and produced an accurate estimated trajectory that matches the GPS points.

2) *Iver-136 Performance:* In contrast to the field trials conducted during October 2016, the DVL on Iver-136 was operational for this field experiment. Although the dynamic model velocity was fused into the CL EKF, the DVL remained available for the IMU EKF. Therefore, the implementation of the IMU-EKF for Iver-136 used both a dynamic model velocity and its DVL. All of the parameter values for the IMU EKF given in Table II remain the same for this implementation except those identified in Table VII. Other experimental speed trials identified that the vehicle reaches a maximum speed of 1.54 m/s instead of its designed rated speed of 2.06 m/s. For this reason, a maximum speed value of 1.54 m/s was used for the coupled range filter.

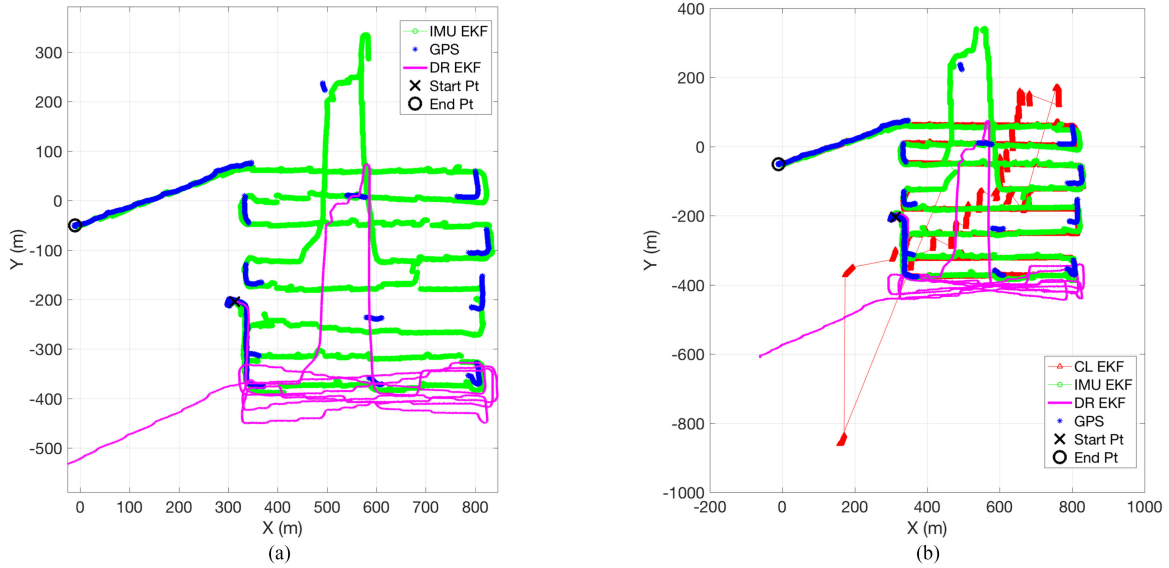


Fig. 8. Iver-106 IMU EKF trajectory plot. The IMU EKF solution (green) and the DR EKF (magenta) plotted against the associated GPS position fixes (blue) for comparison. The DVL-aided CL EKF (red) is plotted for comparison purposes only with the DVL-aided solutions. (a) IMU EKF and DR EKF with the vehicle dynamic model velocity used as its speed measurement. (b) IMU EKF and DR EKF with the DVL used as the speed measurement. Note the difference in the scales between the plots due to the lack of range filtering on the CL EKF solution.

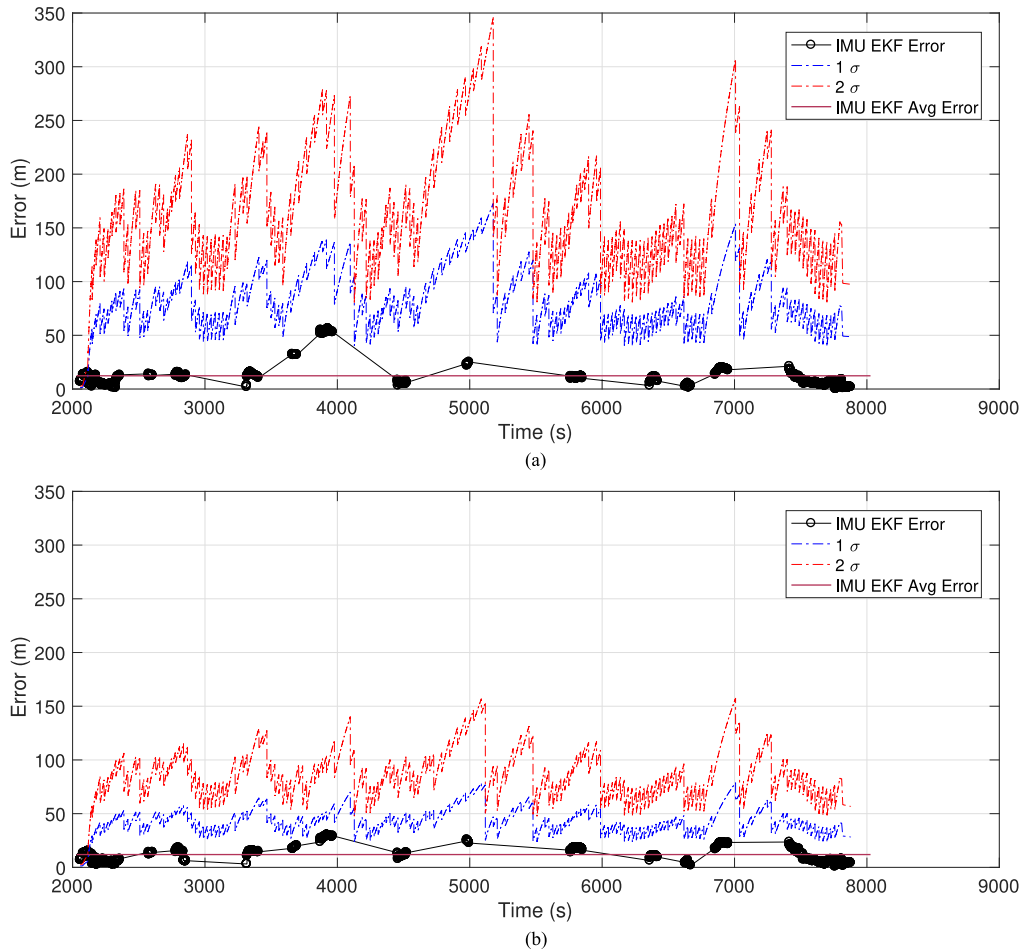


Fig. 9. Iver-106 IMU EKF error summary. (a) IMU EKF error with dynamic model velocity. (b) IMU EKF error with DVL. These plots contain the IMU EKF error (black), its average error (brown), and its associated 1σ (blue) and 2σ (red) uncertainty lines. Note the difference in scales between the two plots; thus showing the DVL-aided solution provided a more accurate estimate.

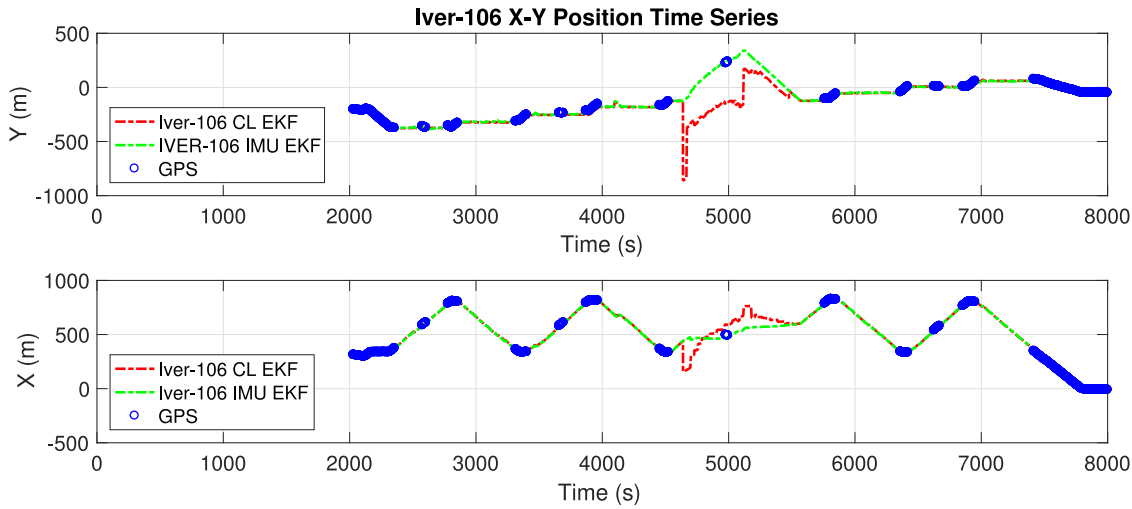


Fig. 10. Iver-106 XY position time-series summary. Position X (bottom) and Y (top) time-series plots of the IMU EKF (green) plotted with the CL EKF (red) and associated GPS position fixes (blue). These plots show the necessity of the coupled range filter to remove the erratic behavior displayed by the CL EKF.

The trajectory summaries for the Iver-136 IMU EKF, using both the dynamic model velocity and the DVL, are displayed in Fig. 11, and the error summaries are shown in Fig. 12. Fig. 11(a) contains the dynamic model velocity aided CL EKF solution for direct comparison purposes. As this plot clearly shows that the erratic behavior exhibited by the CL EKF is clearly removed in the IMU EKF solution. Further analysis of the XY position time-series plot (see Fig. 13) also supports the coupled range filter enhancing solution accuracy by replacing the erratic behavior of the CL EKF at $t = 1000$ s and $t = 4500$ – 5000 s with a smooth stable solution.

The IMU EKF observed its maximum error of approximately 150 m in the first 300 s of the mission during the troubleshooting window of Iver-106. This issue occurred both in the dynamic model velocity aided and DVL-aided scenarios. Iver-136 received and processed a range of 716.1 m at time $t = 286.7$ s, from Iver-106 when its state was not accurate, which resulted in a position shift of Iver-136 to the north to approximate position (500, 300), as shown in Fig. 11. The coupled range filter did not prevent this range from being processed because the time and position of the last update used in the range filter algorithm were the initialization points to the GPS at position (500, −25) at time $t = 0$. A speed of 0.88 m/s was necessary to trip the state-acceptance gate equation to prevent the IMU EKF from processing this range. Due to this initial offset, the position estimates remained to the east of the GPS fixes on the first southern leg [from positions (800, 200) to (725, −190)], but the IMU EKF later converged to the GPS points at approximately 1100 s for both the dynamic model velocity aided and DVL-aided IMU EKF and remained mostly below the 2σ uncertainty curves for the remaining of the mission. The CL EKF did not experience this same issue because it was in constant receipt of the GPS during the first 300 s and therefore was not affected by the poor state estimate from Iver-106.

Table VIII shows the average errors from the GPS for all of the navigation solutions for both Iver-106 and Iver-136. To provide a better comparison, the error values after the CL solution for

TABLE VIII
APRIL 2017 FIELD TRIALS PERFORMANCE SUMMARY. (a) IVER-106.
(b) IVER-136

Solution	DVL-Aided	Model Velocity-Aided
IMU EKF	11.93 m	12.32 m
CL EKF	12.87 m	N/A
DR EKF	283.89 m	257.45 m
Distance Traveled	5.28 km	5.28 km

(a)

Solution	DVL-Aided	Model Velocity-Aided
IMU EKF	24.57 m	32.25 m
CL EKF	N/A	52.86 m
DR EKF	143.19 m	190.09 m
Distance Traveled	6.91 km	6.91 km

(b)

Iver-136 were corrected by the GPS measurements have been removed. As the table shows, the model velocity aided IMU EKF is competitive with the other methods.

The three field trials presented in Section IV provide an extensive analysis of the IMU EKF with the coupled range filter by using three different vehicles executing three different mission trajectories in two different locations. Compared to other navigation methods presented in this paper, the IMU EKF is a competitive alternative to the current approaches.

V. MONTEREY BAY, CALIFORNIA FIELD TRIAL RESULTS

Field data from the 2016 Keck Institute for Space Studies, Pasadena, CA, USA, “Satellites to the Ocean Floor,” research field program [8] served as a final implementation of the IMU EKF. As part of this field program, Iver-136 conducted a mission in Monterey Bay, CA, USA (see Fig. 14), and data gathered during this mission provide the analysis for this paper. Since

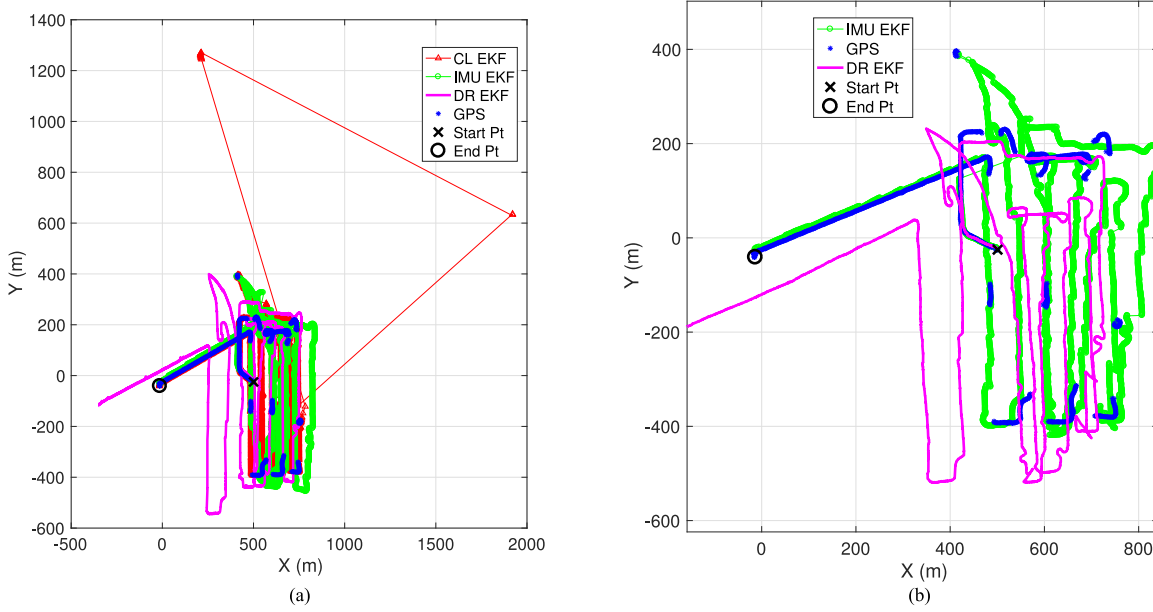


Fig. 11. Iver-136 IMU EKF trajectory summary. (a) IMU EKF with the vehicle dynamic model velocity used as its speed measurement. (b) IMU EKF with the DVL used as the speed measurement. The IMU EKF solution (green) and the DR EKF (magenta) plotted against the associated GPS position fixes (blue) for comparison. (a) is plotted with the CL EKF (red) for a direct comparison. Note the difference in the scales between the plots due to the lack of range filtering on the CL EKF solution.

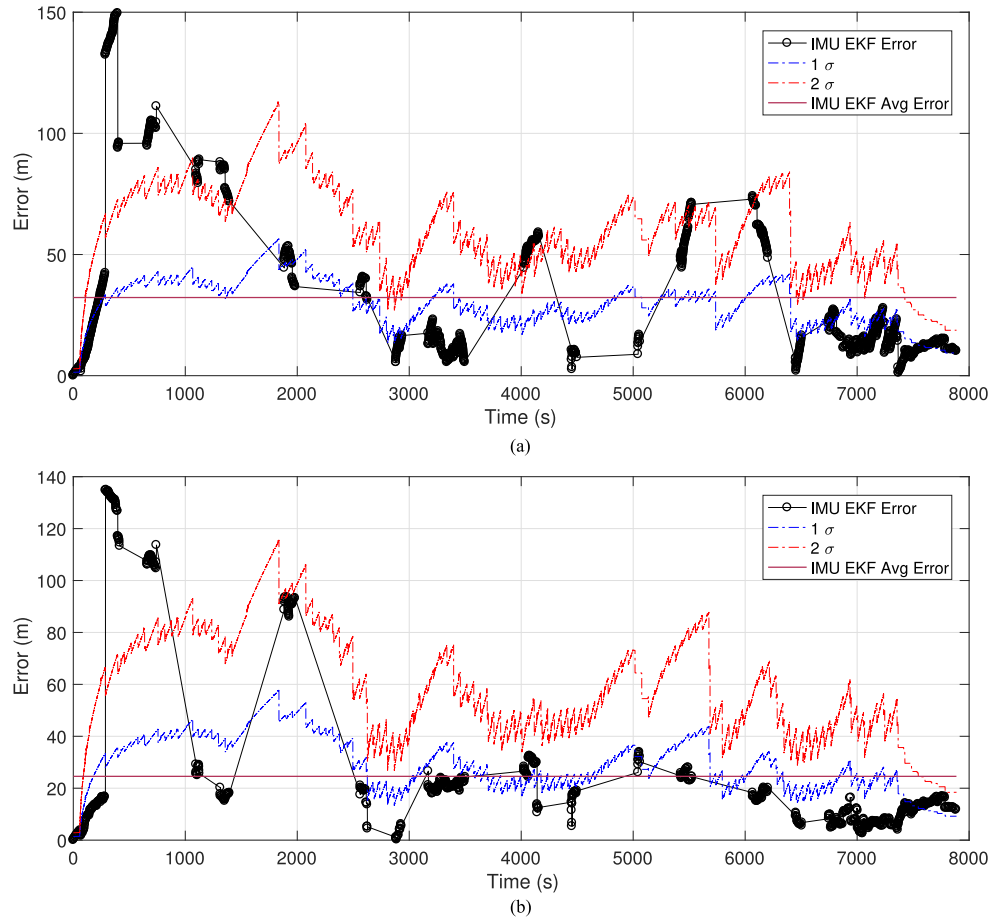


Fig. 12. Iver-136 IMU EKF error summary. (a) IMU EKF error with model velocity as the speed measurement. (b) IMU EKF error with DVL used as the speed measurement. The plots contain the IMU EKF error (black), its average error (brown), and its associated 1 σ (blue) and 2 σ (red) uncertainty lines.

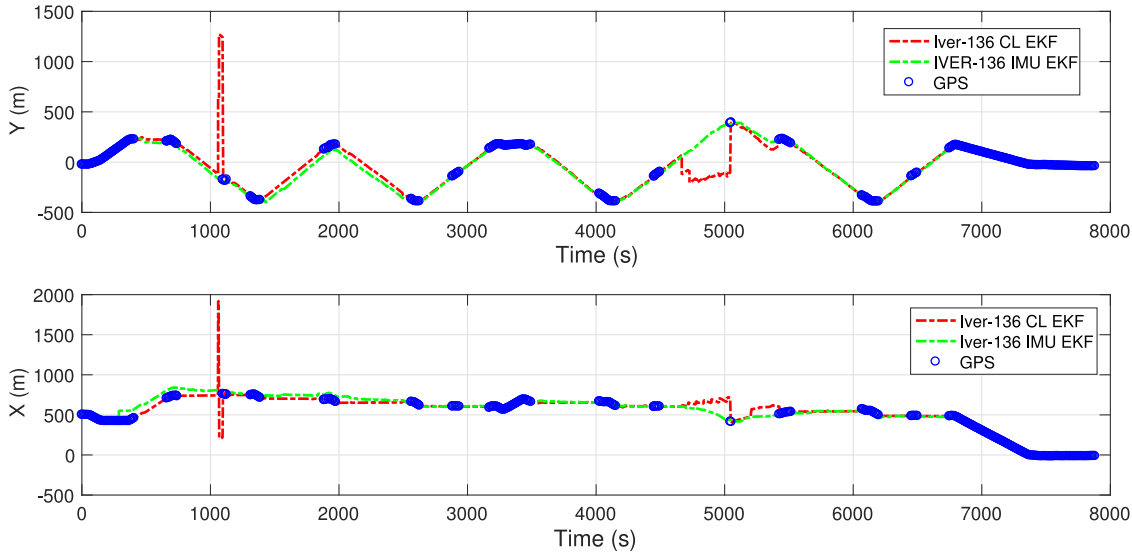


Fig. 13. Iver-136 XY position time-series summary. Position X (bottom) and Y (top) time-series plots of IMU EKF (green) plotted with the CL EKF (red) and associated GPS position fixes (blue). These plots show the necessity of the coupled range filter to remove the erratic behavior displayed by the CL EKF.

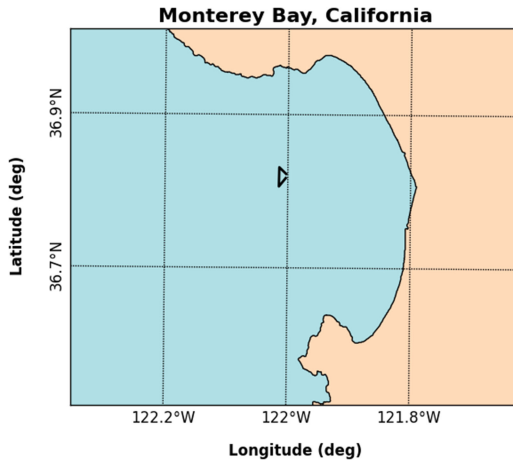


Fig. 14. Monterey Bay, California with position of the Iver-136 mission, identified by the black triangle, during the Keck Institute for Space Studies field program.

one of the focuses of this paper is navigation without a DVL, this field data provide a good assessment of the dynamic model velocity aided IMU EKF implemented on a vehicle operating in strong currents and in water depths where DVL bottom lock is not available.

Since ocean currents are prevalent in Monterey Bay, the addition of a velocity bias estimator similar to one used in a previous work [20] was added to this IMU EKF implementation to improve the accuracy of the model velocity input. In the previous work, as well as other work involving underwater gliders operating in the Arctic Ocean [19], the state updates from the OWTT range measurements provided a means of calculating a water velocity measurement. This water velocity measurement is then processed in a coupled Kalman filter to the navigation state estimator that produces an updated velocity bias. The model velocity measurement incorporates this bias; thus updating it with ocean currents and making it more accurate.

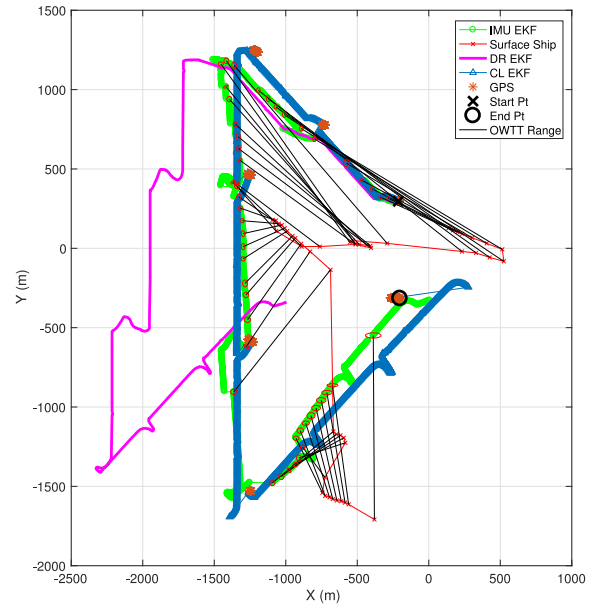


Fig. 15. Iver-136 trajectory summary on Monterey Bay, CA, USA. The following navigation solutions are displayed: IMU EKF (green), CL EKF (light blue), and the DR EKF (magenta). GPS (brown) fixes are displayed for ground truth. The *R/V Shana Rae*, which served as the surface beacon (red), maneuvered throughout the mission to maintain acoustic connectivity. The black lines illustrate the OWTT ranges from the surface beacon to the vehicle, and the red ellipses are the position uncertainties computed by the IMU EKF.

A. Trajectory Summary

During this field survey, Iver-136 operated in a half-bowtie type trajectory, as shown in Fig. 15. This plot shows three solutions for comparison (IMU EKF, DR EKF, and the CL EKF) along with GPS points during the surfacings in the mission. Data were trimmed to the time line of the vehicle's deployment. Since this mission involved a single beacon deployed from the support vessel (and similar to the analysis in Section IV-A), all of the parameters identified in Table II remained the same except the

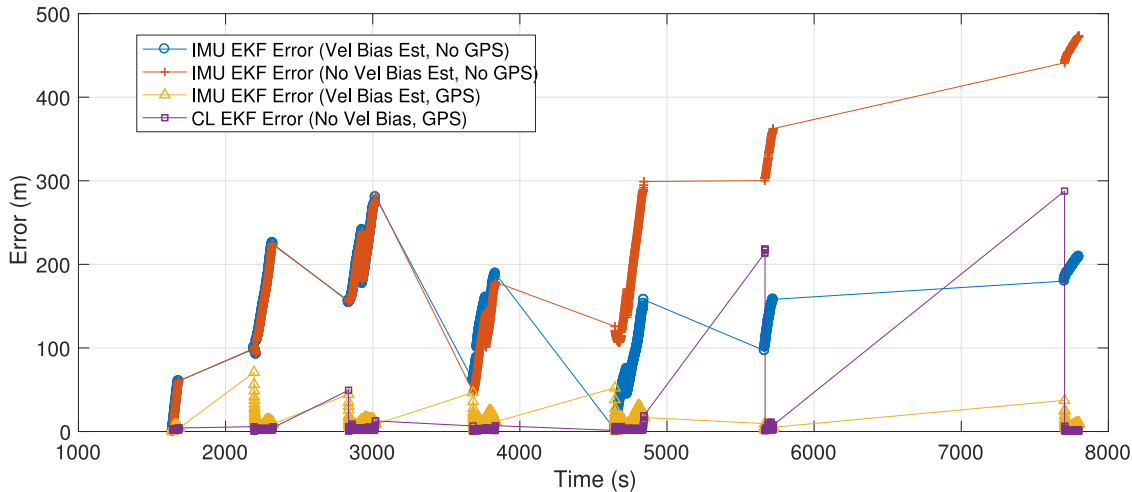


Fig. 16. Iver-136 navigation solution error summary. Navigation solution error compared to the GPS fixes are displayed: IMU EKF with velocity bias estimator (blue), IMU EKF without the velocity bias estimator (red), IMU EKF with velocity bias estimator and GPS (gold), and the CL EKF (purple).

process noise gain factor \tilde{q} was set to 100 versus 1.0. Unlike the previous experiments, the CL EKF solution did not incorporate any OWTT range measurements, but it did process the GPS and used the vehicle's dynamic model velocity for its speed estimation. Also, similar to the implementation on Iver-136 in the previous work [21], the IMU EKF in this implementation used a more accurate model velocity than the one used for the CL EKF.

B. Performance Analysis

The total mission time was approximately 103 min with a total distance of 6.1 km traveled. Like the Ashumet Pond trials, the surface beacon was set to transmit at a frequency of once every 60 s (~ 0.02 Hz). However, Iver-136 only received a total of 49 acoustic packets, equating to an acoustic loss of approximately 52%. Reasons for the high loss rate were due to the *R/V Shana Rae* repositioning during the mission as well as high background noise from its engines; thus lowering the signal-to-noise ratio of the transmitted packets. Nonetheless, since Iver-136 experienced such a high loss rate of its OWTT measurements, the vehicle accrued significantly more error compared to the previous results discussed in Sections IV-A and IV-C.

Fig. 16 shows the error with respect to the GPS position fixes for the various navigation solutions. As shown, because of the high acoustic loss rate, the IMU EKF experienced an average error of approximately 141 m. However, this plot does show the significant effect of the velocity bias estimator. The IMU EKF that incorporated the velocity bias estimator (light blue) outperforms the IMU EKF solution without it (red) by approximately 30%, particularly from $t = 4000$ s to the end of the mission. Additionally, when the IMU EKF processed GPS (gold), it exhibited a better position reset offset as compared to the CL EKF (purple). Particularly, at $t = 5667$ s, the IMU EKF had a position reset of approximately 200 m less than the CL EKF. Likewise, at $t = 7770$ s, the IMU EKF experienced a position reset of approximately 250 m less than the CL EKF.

Overall, the IMU EKF method presents a better alternative to the CL EKF solution.

VI. CONCLUSION

The main goal of this paper was to investigate a navigation solution for AUVs that uses a minimal sensor suite to reduce power consumption and cost, allows applicability throughout the water column, and performs with an acceptable threshold of accuracy. The research presented in this paper proves that a viable option exists which is dependent upon an MEMS IMU for odometry and attitude, a vehicle's dynamic model velocity, and passive acoustic aiding.

In this navigation solution, the vehicle's state was estimated by an EKF that propagated a kinematic constant acceleration model to determine the vehicle's XY position, velocity, and acceleration. This propagated model was augmented by processing measurements of linear accelerations from the MEMS IMU, velocity from propeller motor speed or a DVL, and OWTT range measurements from one or two beacons. In addition, the state estimation included IMU accelerometer bias, which also incorporated bias measurements from the updated state's position after a range measurement. Coupled with the EKF was a range filter that prevented the IMU EKF from processing erroneous OWTT range measurements because of inaccurate clock synchronization between the beacon and the receiver, inaccurate state estimation from the transmitting beacon, or due to various environmental conditions that can affect sound propagation. This range filter prevented the IMU EKF from processing faulty ranges by two processes: a maximum operating range filter and a state-acceptance gate.

The effectiveness of this EKF model was evaluated by implementations on data collected in three different controlled environment field experiments and one open ocean environment. These field experiments included two OceanServer Iver2 AUVs in two separate field trials on Ashumet Pond and one field experiment of a Bluefin Robotics SandShark μ AUV on the Charles River. Each of these exper-

iments incorporated a topside beacon, transmitting its GPS position, whereas the two experiments in Ashumet Pond also incorporated an assessment of intervehicle ranging and multivehicle navigation. These experiments provided a wide spectrum of different vehicles, different acoustic environments, and distinct mission trajectories that assessed the capability of the IMU EKF navigation method. Analysis of these experiments proves that the IMU EKF method gives an average position error on the order of tens of meters over a time scale of about 2 h and a spatial scale of approximately 7 km. Additionally, the use of other vehicles in formation as a transmitting beacon and incorporating bias estimation enhanced the navigation performance. Also, the addition of the coupled range filter was paramount to the IMU EKF's success by preventing faulty range measurements that cause the IMU EKF to become unstable. Finally, an implementation of the IMU EKF in Monterey Bay, CA, USA, proved that this method outperforms other methods in open ocean currents.

This research demonstrates a capability of perfecting low cost low power sensors for accurate navigation is attainable. Future research should incorporate a means to distinguish between velocity and acceleration biases. Additionally, the coupled range filter provides a decision point in the vehicle's navigation algorithm on how to proceed with inaccurate navigation. Future research can include how a vehicle changes its trajectory to improve navigation performance, notifies a human in the loop, or changes its mission to obtain a GPS fix to prevent or minimize instability in its navigation solution. Nonetheless, this navigation solution is applicable to a wide range of platforms. It is beneficial to the emerging μ AUV class and the longer endurance platforms, such as autonomous underwater gliders. Additionally, this solution is attractive for future "master-slave" heterogeneous vehicle deployments, in which a large AUV with a high-end INS serves as a communication and navigation aid to smaller vehicles [57]. These advances in using measurements from inexpensive and low-power sensors to obtain accurate underwater navigation enable new operational paradigms for the oceanographic and military AUV communities.

ACKNOWLEDGMENT

The authors would like to thank S. Suman for his technical expertise and assistance in preparing and conducting field experiments, N. Rykema, E. Fischell, and the MIT LAMSS lab that provided data from the SandShark μ AUV deployment, Dr. B. Hodges for providing Iver-106, and Dr. D. Fratantoni for his assistance with the field experiments. Dr. R. Camilli graciously lent them the surface skiff used in their lake trials. Captain J. Christmann of the *R/V Shana Rae* ably supported their California field work. Dr. S. Webster provided valuable insight and feedback. The views presented in this paper are those of the authors and do not necessarily represent those of the U.S. Department of Defense or the Department of the Navy.

REFERENCES

- [1] J. C. Kinsey, R. M. Eustice, and L. L. Whitcomb, "A survey of underwater vehicle navigation: Recent advances and new challenges," in *Proc. Int. Fed. Autom. Control Conf. Maneuv. Control Mar. Craft*, 2006, vol. 88, pp. 1–12.
- [2] L. Paull, S. Saeedi, M. Seto, and H. Li, "AUV navigation and localization: A review," *IEEE J. Ocean. Eng.*, vol. 39, no. 1, pp. 131–149, Jan. 2014.
- [3] N. Brokloff, "Dead reckoning with an ADCP and current extrapolation," in *Proc. MTS/IEEE OCEANS Conf.*, Halifax, NS, Canada, Oct. 1997, vol. 2, pp. 994–1000.
- [4] L. L. Whitcomb, D. R. Yoerger, and H. Singh, "Advances in Doppler-based navigation of underwater robotic vehicles," in *Proc. IEEE Int. Conf. Robot. Autom.*, Detroit, MI, USA, May 1999, vol. 1, pp. 399–406.
- [5] J. C. Kinsey and L. L. Whitcomb, "Preliminary field experience with the DVNAV integrated navigation system for oceanographic submersibles," *Control Eng. Pract.*, vol. 12, no. 12, pp. 1541–1548, Dec. 2004 (Invited Paper).
- [6] M. M. Hunt, W. M. Marquet, D. A. Moller, K. R. Peal, W. K. Smith, and R. C. Spindel, "An acoustic navigation system," *Appl. Ocean Phys. Eng.*, Woods Hole Oceanograph. Inst., Woods Hole, MA, USA, Tech. Rep. WHOI-74-6, 1974.
- [7] J.-P. Peyronnet, R. Person, and F. Rybicki, "Posidonia 6000: A new long range highly accurate ultra short base line positioning system," in *Proc. OCEANS Conf.*, 1998, vol. 3, pp. 1721–1727.
- [8] A. F. Thompson *et al.*, "Satellites to seafloor: Toward fully autonomous ocean sampling," *Oceanography*, vol. 30, Jun. 2017, pp. 160–168. [Online]. Available: <https://doi.org/10.5670/oceanog.2017.238>
- [9] S. Beaulieu, E. Baker, and C. German, "On the global distribution of hydrothermal vents: One decade later," *EOS Transactions American Geophysical Union*, 2012.
- [10] C. Devey, "Long range exploration," *InterRidge News*, vol. 19, pp. 44–45, 2010.
- [11] C. German, E. Ramirez-Llodra, M. Baker, P. Tyler, and the ChEss Scientific Steering Committee, "Deep-water chemosynthetic research during the Census of Marine Life Decade and beyond: A proposed deep-ocean road map," *PLoS One*, vol. 6, no. 8, 2011, Art. no. e23259.
- [12] R. M. Eustice, H. Singh, and L. L. Whitcomb, "Synchronous-clock, one-way-travel-time acoustic navigation for underwater vehicles," *J. Field Robot.*, vol. 28, no. 1, pp. 121–136, 2011.
- [13] R. M. Eustice, L. L. Whitcomb, H. Singh, and M. Grund, "Recent advances in synchronous-clock one-way-travel-time acoustic navigation," in *Proc. OCEANS Conf.*, 2006, pp. 1–6.
- [14] R. M. Eustice, L. L. Whitcomb, H. Singh, and M. Grund, "Experimental results in synchronous-clock one-way-travel-time acoustic navigation for autonomous underwater vehicles," in *Proc. IEEE Int. Conf. Robot. Autom.*, 2007, pp. 4257–4264.
- [15] J. M. Walls and R. M. Eustice, "Experimental comparison of synchronous-clock cooperative acoustic navigation algorithms," in *Proc. MTS/IEEE OCEANS Conf.*, 2011, pp. 1–7.
- [16] S. E. Webster, R. M. Eustice, C. Murphy, H. Singh, and L. L. Whitcomb, "Toward a platform-independent acoustic communications and navigation system for underwater vehicles," in *Proc. OCEANS Conf.*, 2009, pp. 1–7.
- [17] S. E. Webster, L. L. Whitcomb, and R. Eustice, "Preliminary results in decentralized estimation for single-beacon acoustic underwater navigation," in *Proc. Robot. Sci. Syst. VI*, 2010, pp. 1–8.
- [18] S. E. Webster, R. M. Eustice, H. Singh, and L. L. Whitcomb, "Advances in single-beacon one-way-travel-time acoustic navigation for underwater vehicles," *Int. J. Robot. Res.*, vol. 31, no. 8, pp. 935–950, 2012.
- [19] S. E. Webster, L. E. Freitag, C. M. Lee, and J. I. Gobat, "Towards real-time under-ice acoustic navigation at mesoscale ranges," in *Proc. IEEE Int. Conf. Robot. Autom.*, 2015, pp. 537–544.
- [20] B. Claus, J. H. Kepper, IV, S. Suman, and J. C. Kinsey, "Closed loop one-way-travel-time navigation using low-grade odometry for autonomous underwater vehicles," *J. Field Robot.*, 2018, 35:421–434. [Online]. Available: <https://doi.org/10.1002/rob.21746>
- [21] J. H. Kepper, B. C. Claus, and J. C. Kinsey, "MEMS IMU and one-way-travel-time navigation for autonomous underwater vehicles," in *Proc. OCEANS Conf.*, Jun. 2017, pp. 1–9.
- [22] M. J. Stanway, "Delayed-state sigma point Kalman filters for underwater navigation," in *Proc. IEEE/OES Autonom. Underwater Veh.*, Sep. 2010, pp. 1–9.
- [23] A. T. Gardner and J. A. Collins, "Advancements in high-performance timing for long term underwater experiments: A comparison of chip scale atomic clocks to traditional microprocessor-compensated crystal oscillators," in *Proc. OCEANS Conf.*, 2012, pp. 1–8.
- [24] A. T. Gardner and J. A. Collins, "A second look at chip scale atomic clocks for long term precision timing," in *Proc. MTS/IEEE OCEANS Conf.*, 2016, pp. 1–9.

- [25] E. Wolbrecht *et al.*, "Field testing of moving short-baseline navigation for autonomous underwater vehicles using synchronized acoustic messaging," *J. Field Robot.*, vol. 30, no. 4, pp. 519–535, 2013.
- [26] T. L. Song, "Observability of target tracking with range-only measurements," *IEEE J. Ocean. Eng.*, vol. 24, no. 3, pp. 383–387, Jul. 1999.
- [27] A. S. Gadre and D. J. Stilwell, "Toward underwater navigation based on range measurements from a single location," in *Proc. IEEE Int. Conf. Robot. Autom.*, 2004, vol. 5, pp. 4472–4477.
- [28] A. S. Gadre and D. J. Stilwell, "A complete solution to underwater navigation in the presence of unknown currents based on range measurements from a single location," in *Proc. IEEE/RSJ Int. Conf. Intell. Robots Syst.*, 2005, pp. 1420–1425.
- [29] J. M. Walls, S. M. Chaves, E. Galceran, and R. M. Eustice, "Belief space planning for underwater cooperative localization," in *Proc. IEEE/RSJ Int. Conf. Intell. Robots Syst.*, 2015, pp. 2264–2271.
- [30] A. Bahr, M. R. Walter, and J. J. Leonard, "Consistent cooperative localization," in *Proc. IEEE Int. Conf. Robot. Autom.*, 2009, pp. 3415–3422.
- [31] J. M. Walls, A. G. Cunningham, and R. M. Eustice, "Cooperative localization by factor composition over a faulty low-bandwidth communication channel," in *Proc. IEEE Int. Conf. Robot. Autom.*, 2015, pp. 401–408.
- [32] M. De Agostino, A. M. Manzino, and M. Piras, "Performances comparison of different MEMS-based IMUs," in *Proc. IEEE/ION Position Location Navig. Symp.*, 2010, pp. 187–201.
- [33] M. de Bento, B. Eissfeller, and F. Machado, "How to deal with low performance IMUs in an integrated navigation system: Step by step," in *Proc. 5th ESA Workshop Satell. Navig. Technol. Eur. Workshop GNSS Signals Signal Process.*, 2010, pp. 1–10.
- [34] N. Y. Ko, H. T. Choi, C.-M. Lee, and Y. S. Moon, "Attitude estimation using depth measurement and AHRS data for underwater vehicle navigation," in *Proc. OCEANS Conf.*, 2016, pp. 1–4.
- [35] I.-U. Lee, H. Li, N.-M. Hoang, and J.-M. Lee, "Navigation system development of the underwater vehicles using the GPS/INS sensor fusion," in *Proc. 14th Int. Conf. Control, Autom. Syst.*, 2014, pp. 610–612.
- [36] M. S. Sheijani, A. Gholami, N. Davari, and M. Emami, "Implementation and performance comparison of indirect Kalman filtering approaches for AUV integrated navigation system using low cost IMU," in *Proc. 21st Iranian Conf. Electr. Eng.*, 2013, pp. 1–6.
- [37] F. Dukan and A. J. Sørensen, "Integration filter for APS, DVL, IMU and pressure gauge for underwater vehicles," *IFAC Proc. Vol.*, vol. 46, no. 33, pp. 280–285, 2013.
- [38] D. Titterton and J. L. Weston, *Strapdown Inertial Navigation Technology*. Stevenage, U.K.: Peregrinus, 1997.
- [39] G. Troni and L. L. Whitcomb, "Adaptive estimation of measurement bias in three-dimensional field sensors with angular rate sensors: Theory and comparative experimental evaluation," in *Proc. Robot., Sci. Syst.*, 2013, doi: 10.15607/RSS.2013.IX.050.
- [40] R. Alonso and M. D. Shuster, "TWOSTEP: A fast robust algorithm for attitude-independent magnetometer-bias determination," *J. Astronaut. Sci.*, vol. 50, no. 4, pp. 433–452, 2002.
- [41] J. L. Crassidis, K.-L. Lai, and R. R. Harman, "Real-time attitude-independent three-axis magnetometer calibration," *J. Guid. Control Dyn.*, vol. 28, no. 1, pp. 115–120, 2005.
- [42] A. Benini, A. Mancini, A. Marinelli, and S. Longhi, "A biased extended Kalman filter for indoor localization of a mobile agent using low-cost IMU and UWB wireless sensor network," *IFAC Proc. Vol.*, vol. 45, no. 22, pp. 735–740, 2012.
- [43] D. Unsal and K. Demirbas, "Estimation of deterministic and stochastic IMU error parameters," in *Proc. IEEE/ION Position Location Navig. Symp.*, 2012, pp. 862–868.
- [44] R. E. Kalman, "A new approach to linear filtering and prediction problems," *Trans. ASME-J. Basic Eng.*, vol. 82, no. ser. D, pp. 35–45, 1960.
- [45] L. A. McGee and S. F. Schmidt, "Discovery of the Kalman filter as a practical tool for aerospace and industry," NASA, Washington, DC, USA, NASA TM-86847, 1985.
- [46] M. S. Grewal and A. P. Andrews, *Kalman Filtering: Theory and Practice Using MATLAB*, 2nd ed. New York, NY, USA: Wiley, 2001.
- [47] Y. Bar-Shalom, X. R. Li, and T. Kirubarajan, *Estimation With Applications to Tracking and Navigation: Theory Algorithms and Software*. Hoboken, NJ, USA: Wiley, 2001.
- [48] M. El-Diasty and S. Pagiatakis, "Calibration and stochastic modelling of inertial navigation sensor errors," *J. Global Positioning Syst.*, vol. 7, no. 2, pp. 170–182, 2008.
- [49] W. Flenniken, J. Wall, and D. Bevly, "Characterization of various IMU error sources and the effect on navigation performance," in *Proc. ION GNSS*, 2005, pp. 967–978.
- [50] J. Crowell, "Small AUV for hydrographic applications," in *Proc. OCEANS Conf.*, 2006, pp. 1–6.
- [51] A. Thompson, J. C. Kinsey, M. Coleman, and B. Castano, and s. c.-l. Rebecca, "Satellites to the seafloor: Autonomous science to forge a breakthrough in quantifying the global ocean carbon budget," KECK Inst. Space Stud., California Inst. Technol., Pasadena, CA, USA, Tech. Rep., 2015. [Online]. Available: <http://www.kiss.caltech.edu/study/seafloor>.
- [52] O. A. Viquez, E. M. Fischell, N. R. Rypkema, and H. Schmidt, "Design of a general autonomy payload for low-cost AUV R&D," in *Proc. IEEE/OES Autonom. Underwater Veh.*, 2016, pp. 151–155.
- [53] M. V. Jakuba, J. C. Kinsey, J. W. Partan, and S. E. Webster, "Feasibility of low-power one-way travel-time inverted ultra-short baseline navigation," in *Proc. MTS/IEEE OCEANS Conf.*, 2015, pp. 1–10.
- [54] N. R. Rypkema, E. M. Fischell, and H. Schmidt, "One-way travel-time inverted ultra-short baseline localization for low-cost autonomous underwater vehicles," in *Proc. Int. Conf. Robot. Autom.*, 2017, pp. 4920–4926.
- [55] E. Fischell, T. Schneider, and H. Schmidt, "Design, implementation, and characterization of precision timing for bistatic acoustic data acquisition," *IEEE J. Ocean. Eng.*, vol. 41, no. 3, pp. 583–591, Jul. 2016.
- [56] A. S. Huang, E. Olson, and D. C. Moore, "LCM: Lightweight communications and marshalling," in *Proc. IEEE/RSJ Int. Conf. Intell. Robots Syst.*, 2010, pp. 4057–4062.
- [57] L. E. Freitag, M. Grund, J. Partan, K. Ball, S. Singh, and P. Koski, "Multi-band acoustic modem for the communications and navigation aid AUV," in *Proc. MTS/IEEE OCEANS Conf.*, 2005, pp. 1080–1085.



James H. Kepper, IV (M'17) received the B.S. degree in mechanical engineering from the U.S. Naval Academy, Annapolis, MD, USA, in 2005 and the M.S. degree in oceanographic engineering from the MIT/WHOI Joint Program, Woods Hole Oceanographic Institution, Woods Hole, MA, USA, in 2017.

His research study focused on underwater navigation with low-grade sensors. He is currently an active-duty submarine officer.



Brian C. Claus (S'09–M'10) received the Ph.D. degree in ocean and naval architecture engineering from the Memorial University in Newfoundland, St. John's, NL, Canada, in 2015. His thesis studied the energy efficient navigation methods for autonomous underwater gliders in surface denied regions.

He recently completed the Postdoctoral Scholarship Program from the Department of Applied Ocean Physics and Engineering, Woods Hole Oceanographic Institution, Woods Hole, MA, USA, where he is currently as an adjunct oceanographer. His research interests include surface denied navigation and low-energy propulsion for persistent multivehicle ocean robotics.



James C. Kinsey (S'03–M'07) received the Ph.D. degree in mechanical engineering from Johns Hopkins University, Baltimore, MD, USA, in 2006. His thesis in the Ph.D. degree was on the precise navigation for underwater vehicles.

He is currently a Senior Engineer at the Department of Applied Ocean Physics and Engineering, Woods Hole Oceanographic Institution, Woods Hole, MA, USA. His research interests include navigation and dynamic systems and their applications to marine robotics and oceanography.